BIOPHYSICS

Mechanosensitive nuclear uptake of chemotherapy

Nicholas R. Scott*, Sowon Kang, Sapun H. Parekh*

The nucleus is at the nexus of mechanotransduction and the final barrier for most first line chemotherapeutics. Here, we study the intersection between nuclear-cytoskeletal coupling and chemotherapy nuclear internalization. We find that chronic and acute modulation of intracellular filaments changes nuclear influx of doxorubicin (DOX). Rapid changes in cell strain by disruption of cytoskeletal and nuclear filaments sensitize nuclei to DOX, whereas chronic reduction of cell strain desensitize nuclei to DOX. Extracted nuclei from invasive cancer cells lines from different tissues have distinct nuclear permeability to DOX. Last, we show that mechano-priming of cells by paclitaxel markedly improves DOX nuclear internalization, rationalizing the observed drug synergies. Our findings reveal that nuclear uptake is a critical, previously unquantified aspect of drug resistance. With nuclear permeability to chemotherapy being tunable via modulation of nuclear mechanotransduction, mechano-priming may be useful to help overcome drug resistance in the future.

INTRODUCTION

A multitude of chemotherapeutics require access to the nucleus for a drug to be effective for cancer treatments (*1*), and cancers are known to have multiple defense mechanisms against these cytotoxic molecules. These well-established mechanisms include modulating activity/expression of plasma membrane–associated efflux pumps, increasing activity of DNA repair molecules, plasma membrane lipid modifications, and mutations that alter efficacy of chemotherapies (*2*–*7*). While these mechanisms have been extensively documented in various cancers, little is known—or even proposed—about how the final barrier to nuclear entry, nuclear transport itself, may reduce chemotherapy efficacy. While nuclear transport is a very active field of research, few studies have compared nuclear transport mechanisms to different cells in the body, specifically between different types of cancer cells.

Considering the physiology of cancer, many reasons come to mind about why different cell or tissue types may have different nuclear internalization rates, including, but not limited to, both ECM and cell-imposed mechanical stresses, shape of the nucleus, and possible differences in the number of nuclear pore complexes (NPCs) on the surface of the nucleus (*8*–*10*). We recently published a review pointing to a variety of potential reasons that uptake of various molecular weight (MW) cargos may transit across the nuclear membrane in a manner that is not dominated by typical diffusion (size-based) relations, which could be cell or tissue type specific (*8*).

Doxorubicin (DOX), an anthracycline, is one of the most common broad-scale nuclear-localizing chemotherapies in use today. It is used to treat both adulthood and childhood cancers for breast (*11*) and prostate (*12*) cancers as well as a multitude of other cancers (*13*, *14*). DOX interacts with mammalian cells through multiple mechanisms. The most common mechanism is intercalation of DNA, where DOX inserts between DNA bases and stabilizes its position through hydrogen bonding (*15*). This intercalation results in the breakdown of double-stranded DNA and fragmented nuclei with condensed chromatin, inducing apoptosis (*16*). Another mechanism is the inhibition of topoisomerase II, an enzyme that regulates DNA's superhelical state and unlinks intertwined DNA strands (*17*). When DOX disrupts topoisomerase II by trapping it at the cleavage site, DNA cannot replicate further and cell death occurs (*15*, *18*). Furthermore, when DOX oxidizes to semiquinone and converts back to DOX, it releases free radical reactive oxygen species (*15*). These reactive oxygen species cause oxidative damage in the nucleus, resulting in cleavage or degradation of DNA that induces DNA strand scissions (*15*, *19*). Some cancer cells, however, exhibit multidrug resistance (MDR), where they have broad resistance to multiple nonrelated drugs (30 or multiple aspects of cytotoxicity like DOX, preventing this chemotherapeutic from reaching its final destination—the nucleus). MDR arises from different mechanisms: most commonly overexpression of membrane-bound drug efflux pump and trapping chemotherapies in lysosomal compartments.

Beyond MDRs, a key facet of aggressive cancers is pathologically altered mechanotransduction (*20*, *21*). Mechanotransduction is the translation of mechanical stimuli to biochemical signals, and the participants of this pathway—the extracellular matrix (ECM), cytoskeleton, LINC (linker of nucleoskeleton and cytoskeleton) complex, and the nucleus (*22*)—play roles in transmitting the mechanical stress to the nucleus. In the nucleus, nuclear lamins (specifically lamin A and lamin C) regulate mechanotransduction (*8*), and their deficiency causes impaired nuclear mechanics and nuclear integrity in mechanically stressed tissues (*23*). Lamin A also works with nuclear F-actin (NFA), and a balance of opposing forces between NFA and lamin A contribute to the regulation of the nuclear shape (*24*).

The effect of mechanical stress on drug efficacy in cancer cells is receiving more interest, but studies are few and most focus on whole tumor response, rather than cellular mechanisms. Some studies have found that mechanical stresses reduce the efficacy of chemotherapeutic agents on cancer cells (*25*, *26*), while others have found increasing mechanical stress improved drug efficacy (at the scale of single cells) (*27*). For reports of reduced efficacy, mechanical stress leads to increased cellular contractility and concomitant stiffening of the ECM (*28*). The mechanical stress exerted by cells and the ECM components (mainly collagen and hyaluronan) causes vessel compression and hypoxia, which decreases the efficacy of chemotherapies and nanotherapies (*29*). On the other hand, a study on ovarian cancer cells found that cells that were cultured on rigid

Department of Biomedical Engineering, University of Texas at Austin, Austin, TX 78712, USA.
*Corresponding author. Email: nrscott@utexas.edu (N.R.S.); sparekh@utexas.edu (S.H.P.)

substrates had increased proliferation, and tumor response to standard chemotherapy drugs was directly proportional to the stiffness of the substrate (and the cell). A corresponding increase in MDR protein expression, however, make it difficult to ascribe the positively correlated stress-chemotherapy efficacy as a direct consequence of mechanical malleability of a cell or if the correlation is due to increased expression of resistance genes (*27*). Ultimately, success of therapies such as DOX or cisplatin relies on nuclear entry. While DOX is much smaller than the soft cutoff size for nuclear diffusion, no studies have probed the fundamental influence of mechanical stress on nuclear internalization of chemotherapy.

Here, we measure the mechanosensitivity of chemotherapy (DOX) nuclear internalization via its intrinsic fluorescence. The DOX internalization signal we measure is likely an aggregate of three components: (i) nuclear entrance rate through NPC machinery (notated as transport), (ii) DOX-binding kinetics to the DNA, (iii) DNA repair speed. We find that DOX aggregate internalization may be modified through atypical mechanical stress and strain, which we attempt to parse out in our study. Aggressive cancer cell lines from breast and prostate tissues show distinct DOX internalization rates when comparing purified nuclei of the two cell lines; however, live, intact cells have similar uptake rates. Coming from tissues with different mechanical properties, we reasoned that mechanics could affect nuclear internalization and further explored how different mechanotransduction pathways may affect a cell's DOX nuclear internalization. Disrupting actin, microtubule, or myosin networks significantly sensitizes the nucleus in breast cancer cells to higher rates of DOX internalization, likely due to a decrease in stress transmitted to or exerted on the nucleus, creating a larger, atypical doorway for molecules and interfering with DNA repair due to these cytoskeletal filaments' role on DNA repair. Knocking down lamin A/C expression, which changes nuclear stiffness, also elicits substantial sensitization. Our results suggest that nuclear transport itself is a unaccounted for facet of chemotherapy resistance.

RESULTS

We sought to probe whether tumor eradication by means of nucleus-localizing chemotherapies, such as DOX, was subjected to an additional intracellular barrier: nuclear entry. While DOX is cell membrane permeable over long times and is much smaller than the "soft" cutoff for passive nuclear transport, here, we study the dynamics of its nuclear entry because the nucleus is DOX's ultimate destination. Therefore, we use a strategy to permeabilize the plasma membrane using a low concentration pulse of digitonin (~15 μg/ml) for 8 min. This allows us to bypass the plasma membrane, similarly to past researchers that wished to deliver impermeant molecules into cells (*30*–*33*), which purposefully reduces the impact of various plasma membrane–associated drug resistance mechanisms, such as efflux pumps, plasma membrane lipid modifications, etc. As the nucleus remains intact with this digitonin treatment (*31*–*34*), this method allows us to effectively measure DOX's intrinsic nuclear internalization. As an additional control to demonstrate digitonin's neutralization of plasma membrane drug efflux pumps, we tested a drug efflux pump inhibitor, verapamil, on digitonin-permeabilized MDA-MB-231 (breast) cells and compared it to cells only permeabilized by digitonin for DOX internalization. Verapamil + DOX-treated cells showed even less nuclear DOX fluorescence compared to cells only permeabilized by digitonin (fig. S1). This experiment confirms that the plasma membrane and drug efflux pumps are no longer rate-limiting in our experimental design, allowing us to attribute differences in nuclear DOX signal to nuclear entry. We further verified that pulsed digitonin had minimal effect on the nuclear membrane integrity by using purified nuclei and a 40-kDa dextran as cargo. The dextrans showed no increase in nuclear transport in the presence of digitonin (see movies S1 and S2 and fig. S2). This result is consistent with previous reports that used significantly higher digitonin concentrations and similar incubation times where a maintained nuclear integrity was measured by various other means (*31*–*34*).

Breast and prostate cancer cell lines have similar live-cell DOX nuclear internalization dynamics despite differences in DOX-binding sites

We measured DOX nuclear accumulation via its intrinsic fluorescence intensity over 20 min (Fig. 1A). For these experiments, digitonin was used in conjunction with a cell-impermeant dye [RedDot 2 (RD2)] to mark cells that were successfully permeabilized, outlined in Fig. 1A. Figure 1 (B and C) show time-lapse images of a standard field of view and traces of DOX nuclei fluorescence over time, respectively. The colored traces in Fig. 1C show the average fluorescence intensity of individual nuclei, while the dotted black line is the median from all tracked nuclei at each time over the entire 20-min experiment. Unpermeabilized cells show no nuclear fluorescence intensity increase over a span of 20 min because minimal DOX transits the plasma and nuclear membranes to bind to DNA over this time (see movie S4); therefore, these cells are never included in our analyses for permeabilized cells. Cellular autofluorescence changes due to digitonin permeabilization were also minimal in the span of the 20-min experiment (see movie S3) and thus do not contribute to our DOX signal. Permeabilizing the plasma membrane allows us to focus on nuclear internalization and effectively remove the influence of $efflux_{plasma}$ and $influx_{plasma}$ (Fig. 1D). This assay design made it possible to compare DOX nuclear internalization between aggressive prostate and breast cancer cells and probe how different elements of mechanotransduction affect nuclear uptake of DOX. We note that while the pulsed digitonin permeabilization bypassed plasma membrane barriers for DOX, it also allows numerous soluble intracellular molecules such as adenosine 5′-triphosphate, guanosine 5′-triphosphate, RAN–guanosine diphosphate, and cargo transport molecules to wash out of the cell (*33*), thereby limiting any active transport. This further emphasizes our focus on passive nuclear transport for the internalization of DOX.

We were curious if both invasive MDA-MB-231 (breast) and PC3 (prostate) cells showed similar nuclear entry of DOX, given their different reported median inhibitory concentration (IC_{50}) values. Given cell density differences for the two cell lines at high confluence and potentially different cell membrane composition, the digitonin concentrations for the two cell lines were determined by a digitonin titration study per cell line to achieve 70% permeabilization as is common for permeabilization agents (*35*). We determined that MDA-MB-231 cells required slightly less digitonin than PC3 cells (fig. S3).

Despite disabling the influence of the MDR and plasma membrane barriers for DOX nuclear internalization, we observed considerable heterogeneity in a single field of view in both invasive MDA-MB-231 and PC3 cancer cell lines (Fig. 2B). This

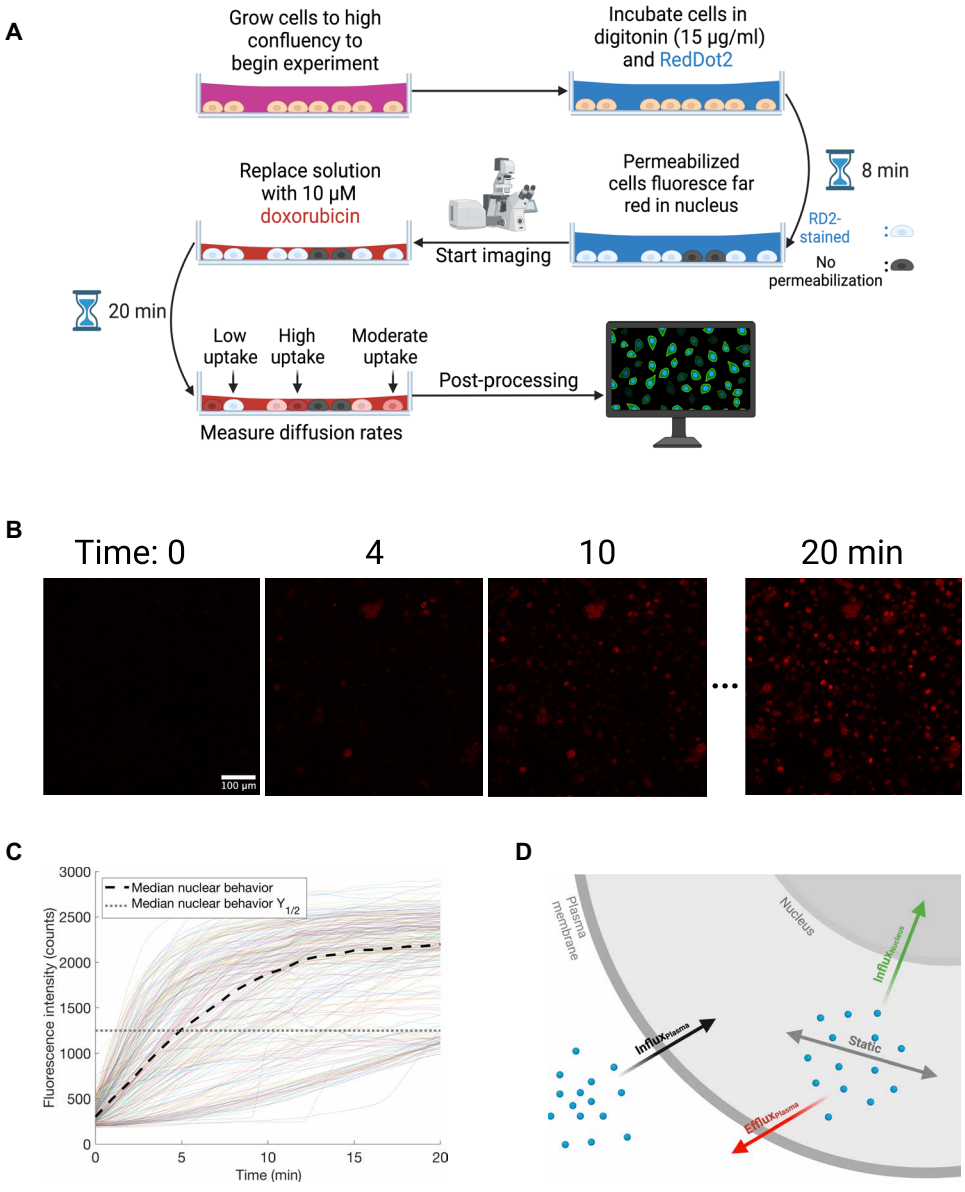

Fig. 1. Experimental overview to measure DOX nuclear internalization in cells. (**A**) Graphical representation of experimental setup. (**B**) Example of a field of view of cells to be analyzed, where the red fluorescence is DOX intercalating into DNA within the nucleus. (**C**) Quantified nuclear DOX fluorescence from permeabilized, where each line is a single nucleus' average intensity tracked over time. The dashed black line is the median behavior of all nuclei in a field of view, individual nuclei curves are used to obtain population statistics, as discussed in further detail in the Supplementary Materials. (**D**) Simplified schematic of the internalization of a chemotherapeutic within a cell where MDR phenomena affect $influx_{plasma}$ and $efflux_{plasma}$ rate variables. Static diffusion is diffusion within the cytosol. In our study, the plasma membrane is perforated to flood the cytosol with DOX, so the dominant aspect measured is $influx_{nucleus}$. (A) and (D) were created in BioRender, and the entire composite figure was compiled in BioRender.

heterogeneity has been reported at double to triple of our concentration of digitonin with even greater permeabilization (*36*) using a different nuclear trafficking probe, indicating that heterogeneity in DOX nuclear internalization we see is a permeabilization or DOX-specific artifact. To our surprise, we found only a slight difference in the median nuclear internalization of DOX for MDA-MB-231 and PC3 (Fig. 2, B and C), where after 20 min, DOX fluorescence in the PC3 median nucleus was slightly greater than MDA-MB-231. We ensured that the average nucleus size is larger than the depth of field of a 0.75 numerical aperture (NA) objective for both cell lines. The depth of field is ~3.08 μm, and the nucleus axial height for either cell line was typically greater than ~7 μm. Therefore, any difference in apparent influx of DOX is not an artifact attributed to focal depth detecting lack of fluorescence outside the nuclei due to nuclei size differences between cells or cell lines. We next looked at cell-to-cell heterogeneity, shown by shading in Fig. 2B. There is slight overlap in these SE (shaded areas) for the two cell lines. A closer look at the heterogeneity of the cells is shown in Fig. 2 (C and D), highlighting cell to cell differences in the intensity range and $V_{Nuclear}$, where each individual nucleus is depicted as a gray dot, with the median

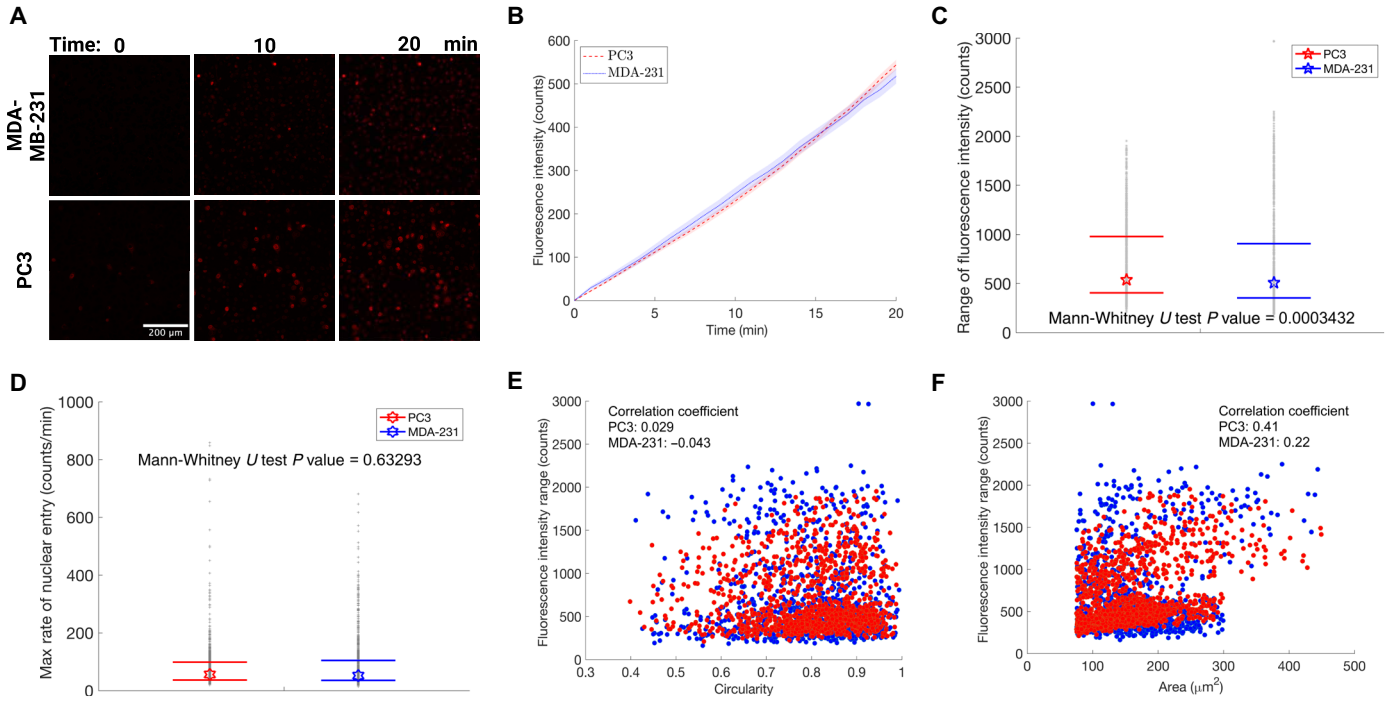

Fig. 2. Different aggressive cancer cells show similar DOX nuclear uptake in live cell studies. (**A**) Representative images of two aggressive cancer cell lines' internalization of DOX over time. (**B**) Quantification of DOX uptake from multiple experiments for the two aggressive cell lines. Median behavior (lines) and standard error (shadows) are shown. (**C**) Distribution of the two cancer cell lines' total uptake of DOX of each individual nucleus measured by fluorescence intensity change over the span of the experiment and (**D**) maximum nuclear entry rate of DOX for cells in an experiment where the medians are marked by a symbol, and the colored dashes above and below the medians are the first and third quartiles. Analysis of (**E**) 2D circularity and (**F**) 2D area versus DOX uptake after 20 min. A low correlation is observed for DOX uptake versus area using correlation range definitions provided by Mukaka (*55*). (A to F) Extract and visualize data from the same experiments, where the number of technical replicates for MDA-MB-231 and PC3 are $N = 4$ and 2, respectively; number of biological replicates for MDA-MB-231 is $n = 736$ cells, and PC3 is $n = 330$ cells. Statistics are displayed in respective panels for non-normal populations. Imaging conditions were identical for all samples. The entire composite figure was compiled in BioRender.

behavior and quartiles marked in color. Despite their apparent similarities, a non-normal population test was used due to multiple subpopulations Fig. 2C, and both cell lines for fluorescence intensity (F.I.) range are considered statistically different, but their maximum nuclear entry rate, referred to as $V_{Nuclear}$, are statistically indistinguishable. We note that fig. S4 depicts PC3 having the same trend of a slightly higher nuclear uptake compared to MDA-MB-231 with a nonreactive Alexa Fluor 488 molecule, showing molecule independence to these transport findings.

We wondered whether our permeabilization agent or perhaps cytosolic dye influx affected the nuclear uptake. When permeabilized with a different permeabilizing agent (streptolysin O) and probed with nonreactive Alexa Fluor 488 dye to examine to molecular entry into the cytosol, we found that the MDA-MB-231 cells' cytosol contained more Alexa Fluor 488 in the cytosol compared to PC3 (fig. S5), yet relative nuclear uptake was slightly higher for PC3 (as for DOX). In another control, when using much higher DOX concentrations, the DOX fluorescence signal in the two cell lines' cytosols were within a SE of each other. Together, these control experiments emphasize that the difference in nuclear internalization of DOX was robust. In addition, these cell lines had similar nuclear volumes, although significantly different overall DOX signal, varying by about 20%, when fixed and fully permeabilized (fig. S6B). We found a similar reduction RD2 signal in PC3 nuclei compared to MDA-MB-231 nuclei. Considering the accessibility of base pairs to which DOX (or RD2) binds may differ between the two cell lines, we would expect that the DOX internalization rates may correspondingly vary if an uptake rate was solely due to the accessible DOX-binding DNA. Therefore, of the three components: (i) nuclear transport, (ii) DOX-binding affinity to the DNA, (iii) DNA repair speed, binding affinity is not the dominant feature but may still have an impact. However, in live cells, no changes in uptake were evident within a 20-min time span. This indicates that live cells have the ability to change uptake rates or throttle nuclear internalization in some fashion.

DOX internalization in purified nuclei shows intrinsic differences in cancer cell nuclear permeability

Purified nuclei were extracted from these cell lines using a commercial mechanical extraction method, where no detergents or proteases were involved, to maintain fidelity of the nuclei. The purified nuclei were then attached to the surface of a polylysine-coated well, similar to a protocol from (*37*), and subjected to DOX directly, without digitonin (because there is no plasma membrane). From these results, we find that purified nuclei take up DOX much faster than for intact cells based on a plateauing signal around 7 min, as expected, because DOX has direct nuclear access without cytosolic "filling" or organelles acting as obstacles, and nuclear volume significantly reduces when nuclei are not connected to the cytoskeleton. We also found that MDA-MB-231–purified nuclei take up more

DOX than PC3-purified nuclei (fig. S7). With both purified nuclei having statistically similar cross-sectional areas (fig. S8), their live-cell counter parts having statistically similar volumes and a 20% difference in DOX-binding DNA (fig. S6; to be discussed in the next paragraph), we would expect at most a 20% difference in DOX uptake. The difference in DOX internalization in purified nuclei from the cell lines was nearly 30% with PC3-purified nuclei taking up 72% of the MDA-MB-231–purified nuclei (fig. S7). Therefore, any discrepancies between the nuclei above 20% appear to be innate biophysical internalization differences. However, as the DOX uptake for purified versus intact cells is reversed for the two cells lines, this indicates that the MDA-MB-231 cells throttle down overall DOX nuclear influx, which further emphasizes the novelty of showing that downstream DOX uptake is affected independently of established MDR barriers.

Seeing this difference in purified nuclei versus live-cell DOX nuclear uptake, we were curious about the differences between MDA-MB-231 and PC3 cells that might be responsible for determining nuclear permeability to DOX. On the basis of previous findings, possible reasons are: (i) nuclear shape, (ii) variations of density of NPCs, and (iii) mechanical stresses the nucleus is subjected to (*8*–*10*). As mentioned above, we verified that it was reasonable to compare these two cell lines based on their nuclear volumes and DNA capacity. We found nearly identical nuclear volumes and a 20% increase in DNA capacity in MDA-MB-231 cells based on both DOX and RD2 dyes (fig. S6, A and B). With these similar nuclear characteristics, we proceeded to ask whether nuclear shape and two-dimensional (2D) area correlated with DOX nuclear uptake. To that end, we analyzed the final DOX fluorescence (uptake) versus 2D nuclear cross-sectional area and 2D circularity (calculated by the minor axis/major axis) of each nuclei with respect to its final fluorescence intensity (Fig. 2, E and F). Counter to what we expected, both cell lines showed a negligible correlation with nuclear circularity, indicating that measurable 2D geometrical changes, such as at the apex of a sharp ellipse, do not facilitate notable changes in uptake. However, purified nuclei show a weak positive correlation for circularity and DOX uptake for both cell lines (see fig. S9), indicating that nuclear uptake of DOX in live cells of both cell lines is modified. Next, looking at the 2D cross-sectional area, we found a weak to moderately positive correlation for both cell lines and their purified nuclei for DOX uptake (see Fig. 2F and fig. S9), so 2D shape was not an indicator of DOX uptake tendencies in either cell line. Together, with clearly faster nuclear internalization into purified MDA-MB-231 compared to PC3 nuclei, similar nuclear volume and neither 2D nuclear circularity nor area having a sizeable impact on DOX fluorescence for both cell lines, it appears that MDA-MB-231 nuclei in cells have a built-in effective nuclear chemoresistance. We surmise that this nuclear throttling of DOX may additionally contribute to the ~3.5-fold lower IC_{50} concentration of PC3 (*38*) compared to that of MDA-MB-231's (*39*), in addition to classical MDR mechanisms. Another potential facet of DOX sensitivity of these two cell lines may be tissue-dependent nucleoporin (Nup) expression and overall NPC composition, which may alter structure and therefore function of the NPC (*40*). However, the extent of how small-molecule transport is modified by Nups (or the NPC) is unknown. Nevertheless, our data show that purified nuclei showed a near 30% difference in DOX nuclear uptake for the two cell lines, when nuclei were not mechanically tethered to any other cellular structures, while the DOX uptake in live cells was within SE of each other. Therefore, we measured the filamentous cytoskeletal actin and microtubule levels found in PC3 and MDA-MB-231 using confocal staining. We found that the amount of actin was statistically different, while microtubules were somewhat similar (fig. S6, C and D). Given that nuclei are tethered to cytoskeletal filaments through which forces are applied to nuclei, we found it prudent to evaluate the correlations between DOX nuclear uptake and mechanotransduction. Previous studies have investigated a similar topic both computationally and experimentally for larger molecules or apoptosis inducing molecules (*41*–*43*).

Reduced substrate stiffness and cell-generated stress throttles DOX nuclear uptake in cells

Studies have shown that the mechanical stresses that a cell experiences will affect the NPC's channel (*44*) and basket (*45*). For example, pore selectivity for a molecule has been computationally predicted to vary with NPC strain (*46*); a highly strained pore may have an abnormally shaped opening, yielding a dysfunctional NPC channel, which then leads to either (i) a unilaterally leakier NPC or (ii) a more selective NPC to one molecule over another, similarly to what Timney *et al.* (*47*) saw in yeast where mutations in FG Nups yielded an increase in transport of different sized molecules in a nonlinear fashion due to a change in structure of the NPC. However, whether such a functional transport difference exists for nuclei experiencing different mechanical stresses has not been empirically verified for a chemotherapeutic such as DOX.

Because MDA-MB-231 cells were more resistant to DOX uptake, based on IC_{50}s (*38*, *39*), we focus on these cells to explore how nuclear mechanotransduction affects DOX nuclear internalization. As a starting point, we probed how substrate compliance affects nuclear internalization. Clearly, tissue culture plastic is much stiffer than native breast tissue. Therefore, we grew MDA-MB-231 cells on a softer substrate that mimicked its original adipose tissue environment to see how tissue mechanics alters DOX uptake, if at all (Fig. 3). These softer substrates are 0.2-kPa stiffness polyacrylamide gels with slightly different surface chemistry compared to the Ibidi chamber slides. Therefore, a direct comparison between Ibidi chamber slides and the Matrigen Softwells must be interpreted with care. A control experiment comparing tissue culture polystyrene (TCPS) within the dish of the Softwell, having the same surface treatment as the Softwell, showed an intermediary reduction in DOX uptake when using an intermediate (8 kPa) stiffness (see Fig. 3C). The result gave us confidence that reducing substrate stiffness reduces DOX uptake both after 24 hours and 5 days of cell spreading.

Cells grown on adipose-tissue mimicking substrates ($E \sim 0.2$ kPa) for 5 to 7 days showed a significant decrease in DOX nuclear uptake compared to those on tissue culture plastic. Even after sixfold longer times, the cells on soft gels did not exhibit similar uptake as cells on tissue culture plastic. This result is consistent with that seen previous in Andreu *et al.* (*42*) and reinforces the idea that a change in cell-compensated stress, which may be translated to the nucleus, changes the overall ability for molecules to enter the nucleus. In addition, the disparity of DOX uptake between the extremes across different fields of view was markedly smaller on soft substrates, showing that heterogeneity in nuclear trafficking was also reduced. However, because growing cells on softer substrates require days, it is plausible that considerable changes in protein expression can transpire. For example, cells are known to have lower lamin levels on softer substrates, as this is seen in vivo in the invading peripheries of tumor

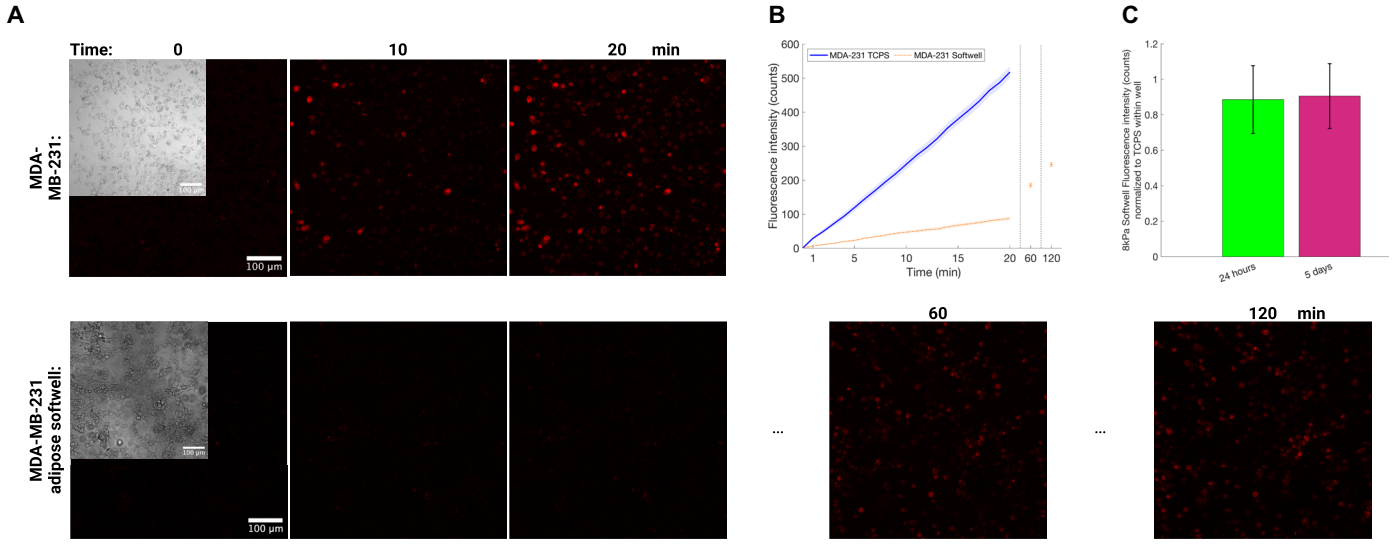

Fig. 3. Culturing cells on soft substrates reduces DOX nuclear uptake. (**A**) Representative images of DOX internalization in MDA-MB-231 on a TCPS or soft substrates, with similar confluence levels around 80 to 90% (shown in bright-field insets on time 0). (**B**) Quantification of many fields of view for 20 min with static time point images at 60 and 120 min for the Softwell. Median behavior (lines) and SE (shadows) are shown. Median is marked by large symbols, colored dashes above and below the medians are the first and third quartiles, and gray points show individual nuclei. For (B), the number of technical replicates (*N*) and biological replicates (*n*) are as follows: MDA-MB-231 TCPS, $N = 6$ and $n = 953$ cells; MDA-MB-231 Softwell, $N = 2$ and $n = 275$ cells. (**C**) Control experiment showing 10 to 12% reduced DOX nuclear internalization for an 8-kPa hydrogel substrate compared to a similarly treated TCPS substrate for 24 hours or 5 days of culture. Bar charts are averages, and error bars are SD error propagation of the populations used to create the ratios. Imaging conditions were identical for all samples. The entire composite figure was compiled in BioRender.

masses (*48*) where the microenvironment has lower stiffness than the tumor core. In addition, lower stresses could also down-regulate stress fibers or perhaps other proteins instrumental in affecting the rate of passive nuclear transport. These factors make it difficult to unequivocally attribute reduced DOX uptake directly to changes in nuclear stress and strain because of cell growth on a softer substrate. However, similarly to the PC3 and MDA-MB-231 circularity analysis, Softwell grown MDA-MB-231's 2D circularity had a negligible correlation to uptake, and 2D area had an even weaker correlation to DOX nuclear uptake than MDA-MB-231 s grown on TCPS (see fig. S10). Therefore, the reduction of DOX uptake was uninfluenced by a change in nucleus size or circularity. In addition, while a tighter distribution of 2D area and circularity existed for Softwell grown cells, the centroid of either TCPS or Softwell populations for circularity and area was very similar.

Acute disruption of cytoskeletal architecture leads to increased DOX nuclear uptake

Therefore, to understand how different aspects of nuclear mechanotransduction contribute to DOX nuclear internalization, we continued an "outside-in" approach, where we acutely perturbed parts of the cytoskeleton using small-molecule inhibitors, and end with a chronic 3-day treatment with knockdown of *LMNA*. These experiments allow us to assess how forces transmitted to the nucleus from the cytosol change DOX permeability of the nucleus (see Fig. 4A for details). Unlike low substrate stiffness experiments, small-molecule inhibitors allow for relatively fast experiments within ~60 min of application to minimize possible changes in off-target protein expression. On the basis of the soft substrate experiment above, we hypothesized that inhibiting the cytoskeleton in some fashion would reduce the mechanical stress that the nucleus experiences through the LINC complex and therefore change the DOX internalization rate. We also found it prudent to ensure cytoskeletal filaments were not destroyed or removed via diffusion out of the cell during the process of permeabilization; therefore, we permeabilized live cells and then paraformaldehyde (PFA)–fixed and stained for actin and microtubules. Cytoskeletal structures were still evident in the permeabilized cells, showing that digitonin use did not destroy cytoskeletal filaments, in agreement with previous research article (see fig. S11) (*32*).

Blebbistatin, latrunculin, nocodazole, and acrylamide are known inhibitors of mechanotransduction pathways that transmit forces to the nucleus via the LINC complex, so mechanical stress reduction to the nucleus is implied when these agents are used (*49*). When looking at Fig. 4 (A and B), we can see that certain the treatments strongly sensitized the cells to DOX. All treatments were previously described in established protocols at given concentrations and incubation times (*50*–*52*). The data indicate that microtubules, actin, nonmuscle myosin II, and even intermediate filaments to some degree play a role in providing nuclear resistance to DOX entry. Acrylamide, which was incubated for 2 hours and should depolymerize intermediate filaments—such as vimentin, keratin, and potentially nuclear lamins (which we test below)—and, to a lesser degree, actin and microtubules, showed only a minor increase in DOX nuclear influx compared to the control. Contrary to the other molecules that had significantly larger effect on DOX nuclear influx, the experiments with acrylamide indicate that intermediate filaments do not strongly influence nuclear uptake of DOX. We note that carrier fluids of these mechano-inhibitors, such as dimethyl sulfoxide, are not relevant during the DOX experiments because the cells are washed thoroughly (five times) during the permeabilization process, flushing any residual molecules of the carrier fluids away before DOX is ever applied to the cells. Cells that were successfully sensitized by disrupting the mechanotransduction pathways of actin or

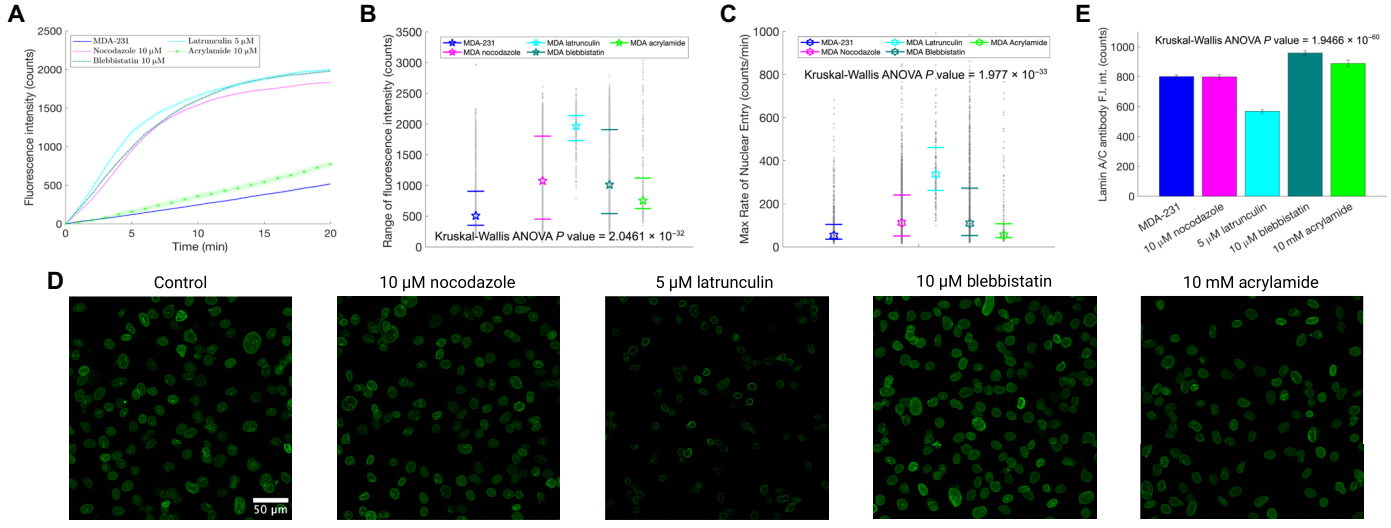

Fig. 4. Rapid disruption of actin, microtubules, or myosin cytoskeletal networks increased DOX nuclear uptake. (**A**) Effect of small-molecule disruption of cytoskeletal filaments on DOX nuclear uptake in MDA-MB-231 cells. Median behavior (lines) and SE (shadows) are shown. (**B**) Distribution of the total DOX uptake of each individual nucleus measured by fluorescence intensity. (**C**) Maximum nuclear entry rate of DOX for cells under the various cytoskeletal inhibitors. Medians are marked by large symbols, colored dashes above and below the medians are the first and third quartiles, and gray points show individual nuclei. For (A) to (C), the number of technical replicates (*N*) and biological replicates (*n*) are as follows: MDA-MB-231, $N = 6$ and $n = 953$ cells; nocodazole, $N = 4$ and $n = 973$ cells; latrunculin, $N = 2$ and $n = 222$ cells, blebbistatin, $N = 4$ and $n = 915$ cells; acrylamide, $N = 2$ and $n = 261$ cells. (**D**) Lamin A/C immunofluorescence images for different treatments and (**E**) fluorescence quantification per cell. Bars are median with error bars showing SE. For (E), the number of technical replicates (*N*) and biological replicates (*n*) are as follows: MDA-MB-231, $N = 4$ and $n = 767$ cells; latrunculin, $N = 3$ and $n = 211$ cells; nocodazole, $N = 2$ and $n = 273$ cells; acrylamide, $N = 1$ and $n = 108$ cells; blebbistatin, $N = 2$ and $n = 308$ cells. Statistics are displayed in respective panels for non-normal populations. ANOVA details are in the Supplementary Materials. Imaging conditions were identical for all samples for DOX and lamin A/C antibody, respectively. The entire composite figure was compiled in BioRender.

microtubules still had a small resistant population that looks similar to untreated cells, as seen in the deconstructed box and whisker plot of DOX (Fig. 4, B and C). The broad distributions of $V_{Nuclear}$ and fluorescence intensity range for the individual nuclei show the heterogeneous population of treated cells. Again, two subpopulations are evident for most treatment types, similar to what was seen in both PC3 and MDA-MB-231 control cells. We recognize that DOX is a complicated and inefficient fluorophore, so we performed this mechano-inhibition coupled with molecule uptake experiment with a different nuclear localizing dye explicitly created to be a fluorophore, RD2. RD2 has roughly double the MW of DOX and has two permanent positive charges (compared to no charge on DOX), and so we deemed it sufficiently different to test whether this mechano-inhibition phenomenon was unique to DOX. Our results show similar sensitization of mechano-inhibited cells occurred with this probe molecule, showing the generality and robustness of this phenomenon (see fig. S12).

While acrylamide is known to affect cytoskeletal intermediate filaments (*52*, *53*), we do not know if it or any of the other small-molecule inhibitors interact with lamin A/C—the intermediate filament nucleoskeleton that supports and anchors the NPC to the nuclear envelope. This is important because if we reduce the stress transmitted to the nucleus and coincidentally reduce nuclear stiffness due to an off-target inhibition of lamin A/C (*23*, *54*), then we would be changing the strain the nucleus and NPCs experience in a convoluted manner. Therefore, we stained all treatment conditions with a lamin A/C antibody after fixing and Triton X-100 permeabilization (Fig. 4, D and E). Lamin A/C antibody staining showed only a mild change in intensity, and the distinct fluorescent thin ring commonly seen around the nuclear envelope appears to be disrupted in only latrunculin dosed cells. Note that while nocodazole, latrunculin, and blebbistatin showed a significant increase from the baseline DOX influx dynamics, they showed only a modest change in lamin signal. Acrylamide-treated cells showed virtually no change in lamin A/C antibody signal or architecture, suggesting that acrylamide does not affect lamin A/C intermediate filaments. In addition, we wished to check whether changes in nuclear area or shape were contributing to the change in influx, perhaps by changing the curvature of the envelope surrounding the NPC (fig. S14). Again, the trends of changes in nuclear area for latrunculin, nocodazole, and blebbistatin treated cells relative to the control cells were inconsistently relative, considering all showed much faster DOX uptake. We further explored how mechano-inhibition treatments possibly changed the correlation coefficients for 2D circularity and area with F.I. All treatments showed a trivial correlation for circularity (<0.15), and a trivial (=0.11) to low (=0.43, 0.44) correlations using correlation range definitions provided by (*55*), depending on the treatment, for area and F.I. (see fig. S13). Therefore, neither differing lamin levels, nuclear shape, nor nuclear area appear to be reasons for the increased DOX influx for the mechano-inhibited cells. In addition, intermediate sensitization was displayed for cells incubated with 0.5 μM latrunculin (fig. S15), which was one-tenth of the concentration shown in Fig. 4. This showed that this sensitization behavior was progressive with a greater reduction of actin stress fibers.

Given the three components that we believe to be the core of nuclear internalization, we wondered if DOX-DNA binding affinity could be altered due to the atypical mechanical stresses after mechano-inhibition. However, we are not aware of any studies

showing DNA structural changes with cytoskeletal inhibition. Therefore, we assume that DOX-DNA binding affinity is not a strongly contributing factor to these mechanosensitive nuclear DOX internalization results.

Silencing of the lamin A/C nucleoskeleton leads to increased DOX nuclear uptake

With changes in cytoskeletal filaments causing changes in DOX nuclear uptake, we moved our focus to the lamin A/C network that supports and anchors the nuclear membrane and NPCs. We knocked down lamin A/C protein expression through small interfering RNA (siRNA) by twofold of the scramble-negative control by using *LMNA* siRNA (Fig. 5, D and E). Immunofluorescence of lamin A/C showed that lamin-specific siRNA resulted in most cells having minimal lamin rings lining the nuclear membrane compared to control or scrambled siRNA treatment. Similar to other treatments, *LMNA* siRNA did not modify the nuclear size (fig. S14). Lamin A/C knockdown elicited a similar sensitization of MDA-MB-231 nuclei in live cells to DOX uptake as was seen for latrunculin, blebbistatin, or nocodazole (Fig. 5, A and B). In addition, no significantly different correlation was evident between circularity or area and DOX uptake compared to other cases (see fig. S16). We believe that lamin expression affects nuclear transport, but it is difficult to compare this with previous cytoskeletal inhibition as the lamin A/C knockdown is not complete. Moreover, lamin A/C inhibition affects nuclear transport in a cargo size-dependent manner. Small molecules such as DOX may experience a modest change in uptake due to large changes in lamin levels, while large molecules (~70 kDa) and exceptionally large molecules (500 kDa) appear to strongly leak into the nucleus that have lamin knockdown (*56*) when they previously were unable to enter the nucleus. These results provide two takeaways: (i) the increase in DOX uptake seen by latrunculin, which happened to have reduced lamin levels, was likely still only due to actin inhibition, as the changes to lamin (Fig. 4E) were similar to that of the siRNA Scramble seen in (Fig. 5E), where DOX nuclear uptake in the siRNA scramble was similar to control MDA-MB-231 cells, and (ii) NPC support/function is unaffected by an almost 25% reduction of lamin A/C by the scramble siRNA but is affected by a reduction in slightly more than 50%. This 50% reduction implies that lamin A/C–binding sites for specific lamin-interacting Nups of the NPC are not limiting transport due to a lack of lamin protein-binding sites—as this would result in a lower uptake rate with fewer gateways into the nucleus for a reduction of lamin A/C. Instead, we believe that the inhibition of lamin A/C yields a reduction in stiffness of the nuclear membrane, leading to a higher membrane strain for a given stress that appears to enhance transport for small molecules. As with cytoskeletal inhibition in live cell, no evidence suggests that DOX-DNA binding nor DNA repair speed are changed with altered lamin levels, suggesting that these are not strong contributors to our results.

Actin and microtubule filament inhibition oppositely affect DOX uptake in purified nuclei

Considering how latrunculin changes uptake rates of DOX within MDA-MB-231, multiple possibilities exist. One possibility is disruption of NFA, while another is elimination of cell-generated stress onto the nucleus by disruption of cytosolic actin filaments connected

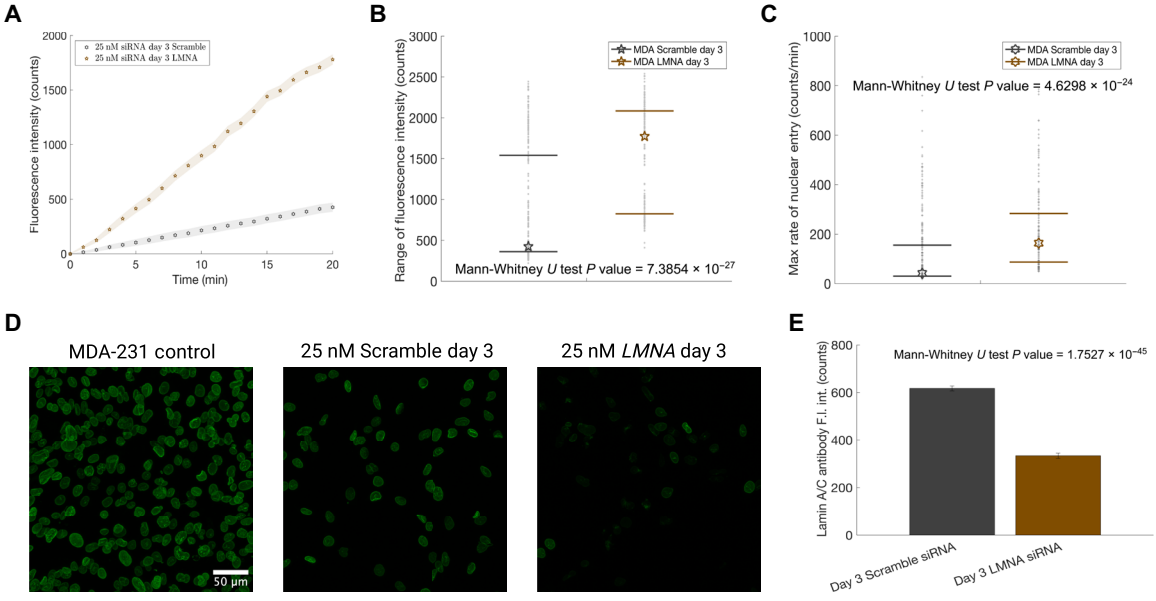

Fig. 5. Lamin A/C knockdown affects DOX nuclear uptake. (**A**) DOX uptake median response for MDA-MB-231 and siRNA scramble and *LMNA* at 25 nM siRNA duplex. Median behavior (lines) and standard error (shadows) are shown. (**B**) Distribution of total DOX uptake of individual nuclei for scramble and LMNA siRNA treatment in MDA-MB-231 cells as measured by fluorescence intensity. (**C**) Maximum nuclear entry rate of DOX for cells with scramble and *LMNA* siRNA treatment in MDA-MB-231 cells. Median is marked by large symbol, colored dashes above and below the medians are the first and third quartiles, and gray points show individual nuclei. For (A) to (C), the number of technical (*N*) and biological replicates (*n*) are as follows: siRNA Scramble, $N = 2$ and $n = 305$ cells; siRNA LMNA, $N = 2$ and $n = 184$ cells. (**D**) Lamin A/C immunofluorescence images for control, scramble siRNA, and *LMNA* siRNA. (**E**) Lamin A/C antibody quantification per cell. Bars are median with error bars showing SE. The number of technical replicates (*N*) and biological replicates (*n*) are as follows: SiRNA Scramble, $N = 3$ and $n = 199$ cells; siRNA *LMNA*, $N = 5$ and $n = 196$ cells. Statistical quantification is displayed in respective panels for non-normal populations. Imaging conditions were identical for all samples for DOX and lamin A/C antibody, respectively. The entire composite figure was compiled in BioRender.

to the LINC complex. NFA resists nuclear deformation (*57*), and Hoffman *et al.* (*44*) showed a colocalization of actin stress fibers and NPC after a cells experience mechanical stress. Perhaps, the inhibition of actin allows for a less discriminant molecular passage by reducing ability for the nucleus to resist deformation? NFA does appear to occur more readily after cells have been subjected to chemotherapies (*57*), which possibly factors into this chemoprotection mechanism. We stained for NFA in live cells and saw a filament network present by colocalized phalloidin staining with DNA staining on a confocal z-stack (see Fig. 6C). To probe the effect of NFA without the complication of the LINC complex and cytosolic-based filaments of the cytoskeleton, we again return to extracted nuclei.

NFA was visible in some purified nuclei with phalloidin staining, but the protein organization was distinct from live-cell NFA (Fig. 6, B and C). In addition, we expect there to be varying degrees of NFA across all cells in a field of view based on the cell cycle and other cell stressors (*57*). Therefore, latrunculin was used to depolymerize NFA in purified nuclei to attempt to highlight the effect of NFA on DOX nuclear uptake. Purified nuclei do not show consistent a NFA network as is seen in live cells; most do not have any evidence of NFA (Fig. 6E and fig. S18). Green aggregates of phalloidin surround the region around nuclei, but little green signal is colocalized within/to nuclei. We originally thought that these aggregates were actin debris from cells; however, after incubating purified nuclei with latrunculin for the same duration that live cells were incubated and then staining for actin, the aggregations were still evident. This meant that it was more likely that phalloidin was aggregating on the polylysine-coated cover glass used to attach purified nuclei for imaging (fig. S18). Nevertheless, purified nuclei were dosed with 5-μm latrunculin for the same amount of time as live cells before incubating the purified nuclei with DOX (Fig. 6A). This experiment showed a minimal increase in DOX nuclear relative to untreated purified nuclei nor a change to heterogeneity. While latrunculin depolymerizes NFA (*57*) to reduce nuclear mechanical deformation, it can have other effects: (1) as a small molecule, it can also enter the nucleus and contribute to nuclear crowding that might restrict DOX entrance or (2) it may somehow interfere with DOX internalization through the nuclear membrane by crowding at the NPCs. We are unable to pinpoint the exact reason why latrunculin-treated purified nuclei show similar DOX uptake to untreated purified nuclei. However, we wished to compare this to the two additional mechano-inhibitors that had large live-cell sensitizations: blebbistatin and nocodazole. Therefore, we measured the effect of blebbistatin and nocodazole on DOX uptake in purified MDA-MB-231 nuclei. We found that nocodazole caused a considerable reduction in DOX uptake compared to untreated, purified nuclei. Because there are no reported microtubules in nuclei not undergoing mitosis, it is possible that nocodazole may interfere similarly to latrunculin (during the 1-hour incubation phase), inhibiting DOX's entrance into the nucleus compared to untreated nuclei. For blebbistatin, DOX internalization in the purified nuclei was slightly reduced compared to untreated, purified nuclei. Because NFA has been shown to contain nonmuscle myosin II, blebbistatin may relieve NFA tension (increasing DOX internalization) while also interfering with NPC transport (inhibiting DOX internalization), resulting in slightly reduced DOX internalization into purified nuclei. To verify that blebbistatin may be crowding the nucleus or NPCs, we measured its intrinsic fluorescence in purified nuclei. Blebbistatin colocalized with the RD2 (fig. S19), which supports the idea that it could crowd the nucleus and disrupt nuclear transport. However, these hypotheses require future study. Last, we note that the multipopulation phenomenon with respect to nuclear area and circularity and DOX uptake that exists in live cells is never present for the purified nuclei (see figs. S9 and S17). All MDA-MB-231–purified nuclei, control or with inhibitors, showed a low positive correlation between DOX F.I. and circularity, while live cells always had minimal correlations.

Subpopulation analysis of cytoskeletal or lamin A/C inhibition reveals multiple routes for DOX nuclear sensitization

A cluster analysis of similar cells within the circularity and F.I. scatter graph revealed treatment-dependent behavior. Looking back to Fig. 2 (E and F), one can easily pick out two different clusters of cells for each cell line. We clustered the cells based on Gaussian fits of the scatter plots and analyzed the trends in circularity, area, uptake, and uptake speed of the slow and fast DOX uptake populations (see fig. S20 and Supplementary Materials for more detail regarding how clustering was done and raw data points). Latrunculin, blebbistatin, and *LMNA* siRNA treatments changed the population such that the slow DOX nuclear uptake population (presumably the more resilient population to DOX) percentage was reduced, while the population that take up DOX faster increased relative to the control. In addition, both cell subpopulations showed faster average DOX uptake speed compared to the control's subpopulations. Overall, the percentage of cells that were fast versus slow in control cells was inverted for cells treated with siRNA *LMNA*, blebbistatin, and latrunculin. We observed almost no change in the DOX uptake population percentages for nocodazole or acrylamide treatment, although uptake speeds of the subpopulations did change. This suggests that the resiliency of the overall cell population may decrease with an acute inhibition of these filament types, where each cytoskeletal filament could be used to biophysically overcome chemotherapeutic resistances, by either shifting the overall population behavior (depicted by shifts in percentage of cells in each subpopulation seen in fig. S20D) to be more rapidly susceptible to DOX or by causing the more resilient, slow uptaking population to end up accumulating more DOX (depicted by shifts in slow cluster's uptake of DOX seen in fig. S20C).

While we tested the effects of how different mechano-inhibitors affected nuclear uptake, we also continuously monitored the correlations between area and circularity as well as DOX uptake measured by change in F.I. Neither circularity nor area changed significantly between MDA-MB-231–untreated cells and mechano-inhibited cells, indicating that the change in DOX uptake was not due to changes to area or circularity. Instead, the commonality between the different cytoskeletal filaments and lamin A/C, all of which sensitized the cells to uptake of not only DOX, but different nuclear localizing fluorophores, was an acute change in strain to the nuclear membrane. While inhibition of any cytoskeletal filament type would reduce mechanical stress transmission to the nucleus, the reduction in nuclear stiffness due to a reduction in lamin A/C functionally affects uptake as well. However, a change in lamin A/C, in theory, should not change mechanical stress transmitted to the nucleus. Instead, it would increase the amount of mechanical strain the membrane experiences. Oddly, these two treatment conditions end up resulting in conflicting mechanical strain changes, where loss of lamin leads to increased strain, while loss of cytoskeletal filaments leads to reduced strain. Therefore, we propose that any acute perturbations

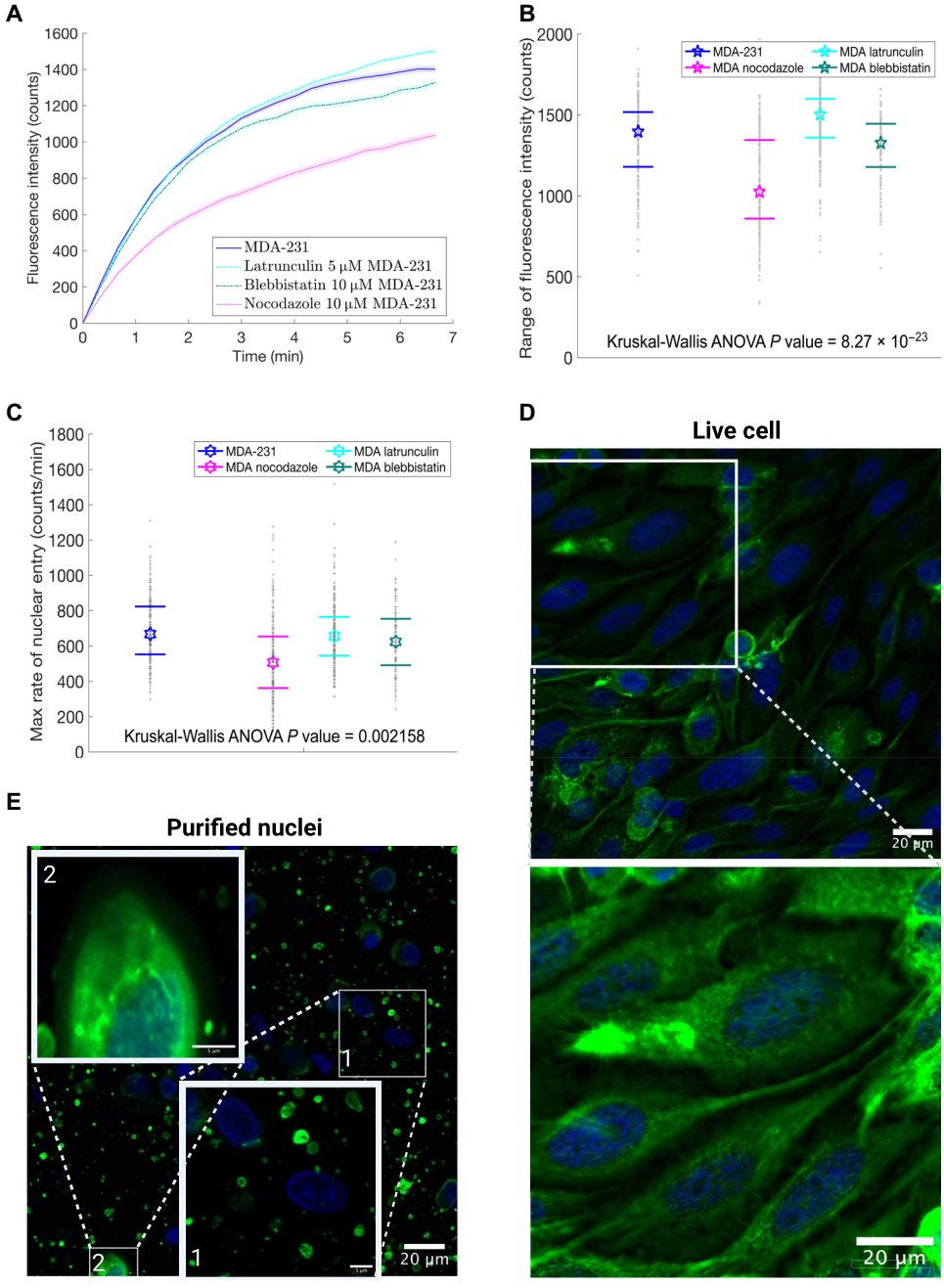

Fig. 6. Purified nuclei of MDA-MB-231 treated with same cytoskeletal inhibition drugs as for cells. (**A**) Purified nuclei show limited change in DOX uptake for with inhibition of actin (latrunculin) or myosin (blebbistatin) activity, but DOX internalization is slowed after nocodazole (microtubule) treatment. Median behavior (lines) and SE (shadows) are shown. (**B**) Distribution of total DOX uptake of individual nuclei for mechano-inhibited purified nuclei of MDA-MB-231 cell line as measured by fluorescence intensity. (**C**) Maximum nuclear entry rate of DOX for cells for mechano-inhibited purified nuclei of MDA-MB-231 cell line. Median is marked by large symbol, colored dashes above and below the medians are the first and third quartiles, and gray points show individual nuclei. The number of technical replicates of (A) to (C) (*N*) and biological replicates (*n*) are as follows: MDA-MB-231, $N = 5$ and $n = 217$ purified nuclei; latrunculin, $N = 4$ and $n = 270$ purified nuclei; blebbistatin, $N = 1$ and $n = 119$ purified nuclei; nocodazole, $N = 2$ and $n = 230$ purified nuclei. (**D**) Live cells and their inset show consistent NFA in all cells. Images in (B) and (C) show phalloidin (green) and DRAQ5 for the nucleus (blue). (**E**) Purified nuclei show heterogenous display of actin in insets (1) where few to none are colocalized with the nucleus and (2) significant amounts are colocalized. Standalone green aggregates in purified nuclei are not actin-specific cellular debris, but instead nonspecific interactions of phalloidin with the surface and general cell debris (see fig. S18 for more details) that can be seen in bright field. Imaging conditions were identical for all samples for DOX, phalloidin, and DRAQ5. The entire composite figure was compiled in BioRender.

that modify nuclear strain [or strain directly imposed on the nucleus directly as in (*42*)] positively affect DOX uptake through changes in the structure and therefore functionality of the NPC, as was theorized in (*45*, *46*). However, allowing for a cell-controlled reduction of nuclear strain by changing cytoskeletal architecture and in expression levels due to a chronic perturbation, e.g., a reduction in substrate stiffness, leads to a reduction in nuclear uptake. With this proposed mechanism, we still are in complete congruence to previous work such as (*42*) that discuss mechano-sensitivity and its relation to nuclear uptake, but we enrich the understanding of this coupled phenomenon with the inclusion of timescales that allow for cells to compensate or not. In addition, this phenomenon does not appear to be substrate stiffness-restricted phenomenon. While we tested the effects of substrate stiffness, we also tested cytoskeletal inhibition, both of which changed uptake. Previous researched pressed on cells (*42*), while others sensitized cells with a shearing flow rate (*43*) that sensitized two different cell lines to an apoptosis-inducing ligand. Therefore, this seems to be a global response in how external mechanical stresses can modify how a cell responds to drugs. Our work highlights that the nucleus itself appears to be instrumental for DOX internalization, but more importantly timescale is extraordinarily important.

Paclitaxel microtubule stabilization demonstrates DOX-paclitaxel synergy

Our findings suggest a rationale for the synergistic effects of a popular combinatorial chemotherapy treatment: DOX and paclitaxel. Paclitaxel's mechanism of action involves the stabilization of β-microtubules (*58*) to prevent cell division. Paclitaxel has also been shown to stiffen both the plasma membrane and intracellular environment through atomic force microscopy and microrheology in different mesenchymal and cancer cell lines (*59*, *60*). Moreover, paclitaxel was recently shown to cause nuclei fragmentation by rigid microtubules squeezing nuclei in malignant ovarian cancer cells (*61*). As administration of paclitaxel is a not a cell-controlled change in stress transmission to the nucleus, we would expect that atypical strains on the NPC would create a leakier sieve pore. We tested our hypothesis regarding synergistic effects of the two drugs with nuclear uptake of DOX as the readout. To avoid excess cell toxicity, we used a 1- and 24-hour incubation at an IC_{90} for MDA-MB-231s (*62*) to see if and how the process yielded changes in nuclear uptake.

Stabilization of the microtubules through 24-hour paclitaxel incubation strongly increased nuclear uptake of DOX (Fig. 7, A to C), similar to how the mechano-inhibition had four- to sixfold sensitization. This confirms our hypothesis that the synergistic effects of these two chemotherapies have resulted in a nuclear sensitization, similar to the other non-cell–compensated perturbations to mechanotransduction pathways. Moreover, the results also reinforce our theory that any acute (stress above or below the baseline stress a cell normally experiences) can affect uptake. Our previous experiments performed induced rapid depolymerization, while paclitaxel does the exact opposite and both markedly improved nuclear uptake of DOX.

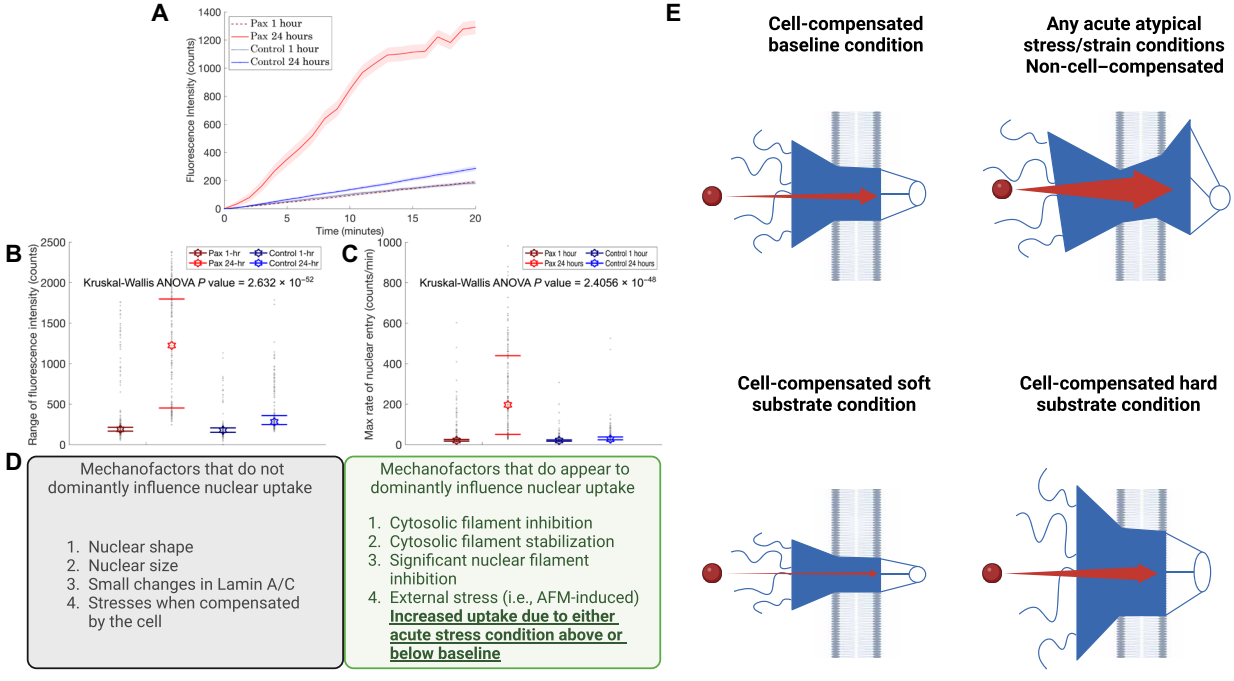

Fig. 7. Mechanotransduction affects nuclear internalization, whether through stabilization or inhibition. (**A** to **C**) MDA-MB-231 cells incubated 24 hours with paclitaxel before nuclear uptake study with DOX to prove that any acute treatment, whether depolymerization or stabilization with positively sensitize cells to DOX. (**D**) Mechanofactors that do and do not affect nuclear uptake based on findings of this study and (*42*). (**E**) Cartoonish depiction of NPCs under various loading conditions whether cell-compensated or not, where the hard substrate cell-compensated (chronic) condition was gleaned from data of a different research paper (*42*). Number of technical replicates (*N*) and biological replicates (*n*) are as follows: MDA-MB-231 1-hour control, $N = 1$ and $n = 224$ cells; MDA-MB-231 24-hour control, $N = 1$ and $n = 252$ cells; paclitaxel 1-hour control, $N = 3$ and $n = 716$ cells; paclitaxel 24-hour control, $N = 3$ and $n = 217$ cells. (D) and (E) were created in BioRender, and the entire composite figure was compiled in BioRender.

DISCUSSION

While it is plausible to ask if rapid changes in nuclear strain affect the porosity of the nuclear envelope itself to modify DOX internalization, recent work showed that all nuclear traffic, regardless of size, goes via NPCs (*63*). Therefore, we believe modified DOX internalization is more likely dominated by molecules passing through atypically deformed NPCs, as was previously purported by researchers (*44*–*46*), in addition to possible reductions in DNA repair accessibility after actin, mysoin, microtubules, or lamin A/C filamentous networks have been disrupted (*64*–*67*). A functional effect on tumor volume reduction was shown in mice when DOX was given to mice with a polymerizing or depolymerizing agent, showing that what we have seen is not necessarily an artifact of in vitro work. Figure 7E is a schematic depicting how a cell-compensated (regulated) mechanical stimulus and noncompensated mechanical stimuli affect transport of DOX through NPCs, altering the total observed internalization. This explanation is fully consistent with the synergy we observed between DOX and paclitaxel, which is also observed at the patient level in bonafide cancer treatment by elevated complete and partial response rates of tumors (*68*).

In addition, we have found that cell cycle is a contributor to DOX and RD2 uptake in preliminary work, where G_2-M cells internalized around 20 to 30% more, on average, than G_1 cells. Cell cycle in a nonsynchronized population of cells may contribute to heterogeneity seen in all populations tested. This may also explain to some degree the shift in population percentages to a phenotype showing increased DOX uptake (seen in fig. S20) for mechano-inhibitors, which are known to arrest cells in a certain cell-cycle phase, such as paclitaxel.

In this study, we found that nuclear uptake of DOX into live cells of two aggressive cancer cell lines from different tissues was notably similar, considering that their IC_{50} values are different by more than threefold. When exploring if there is a fundamental difference of the nuclei themselves by analyzing mechanically separated purified nuclei, we found that the nuclear permeabilities of DOX in the MDA-MB-231 and PC3 cell lines were unique, suggestive of a previously unquantified nuclear barrier to DOX chemotherapy that is independent of established MDR mechanisms. We used this purified nuclei study between these two cell lines as a springboard to explore how these differences are muted in live cells. Specifically, in purified nuclei, the cells have minimal external forces transmitted to the nucleus. Live cells from two different cell lines may have a differing degree of cytoskeletal filament assembly and possibly lamin network assembly, which can modify the strain felt by nuclei within cells. Therefore, we explored whether modifying mechanical stresses would make MDA-MB-231 cells react differently to nuclear internalization of DOX.

Lowering mechanical stress by growing MDA-MB-231 cells on soft substrates (over days) reduced the uptake of DOX, with even sixfold more time not being enough to reach the median uptake of the cells on tissue culture plastic. However, reaching conclusions from a complex scenario such as chronic cultivation on a lower substrate stiffness is difficult due to many conflating cellular changes over this experimental time period, including changes in mechanotransduction gene expression (*69*). We then used an acute perturbation of mechanotransduction by inhibiting microtubules, actin, or myosin II, which resulted in a significant increase of nuclear internalization of DOX in live cells. Along similar lines, siRNA knockdown of *LMNA* resulted in increased DOX uptake, consistent with previous work (*56*). These results all point toward a mechanosensitization of chemotherapy internalization to the nucleus, provided that the mechanical perturbation was acute.

As a final experiment, we used combinatorial therapy now used in cancer therapy: paclitaxel plus DOX. We measured DOX uptake within cells incubated with 24-hour paclitaxel. We saw a sixfold sensitization of DOX. This paclitaxel-DOX synergy is consistent with treatment plans used within patients, indicating that what we see may be happening in vivo. Thus, all of the mechanotransduction pathway perturbations point to a model where a sudden, forced change in nuclear mechanical strain has a sensitization effect on nuclear internalization of DOX, whether by perturbation of cytoskeletal or nucleoskeletal filaments (Fig. 7E). Our findings may help rationalize the existence of a higher NFA expression in cells that have been incubated with a chemotherapy, as part of this newly proposed nucleo-centric chemoprotectant mechanism since NFA has been stated to reduce deformation and thus reduce mechanical strain (*57*).

Lastly, we believe that this work may give more insight as to why certain tissue types seem to be less susceptible to specific chemotherapeutics and/or having a lower therapeutic index ratio for cancer cells to healthy cells, beyond classical MDR mechanisms. As different tissue types experience different levels of mechanical stress, potentially changing NPC function.

MATERIALS AND METHODS

Digitonin and DOX stock solution preparation

Digitonin (Millipore, catalog no. 300410) was prepared in cell culture grade H_2O (autoclaved UltraPure Type 1) and sterile filtered at a concentration of 10 mg/ml as solubility in water is around 50 mg/ml and was aliquoted to be stored at −20°C to avoid freeze thaws. Working concentrations of digitonin were 15 μg/ml for both PC3 and MDA-MB-231, and a solution of that concentration and a RD2 (Biotium, catalog no. 40061) dilution ratio of 1:200 should be prepared before experimentation. In addition, DOX (TCI chemicals, catalog no. D4193) was dissolved in culture grade H_2O at a concentration of 10 μM for 10× the IC_{50} of MDA-MB-231 to be able to see rapid fluorescence intensity increase in the short permeabilization window of 20 min. DOX should also be aliquoted at a higher concentration than working and stored in the freezer for single use purposes as well.

For digitonin permeabilization:

1) Normal media is replaced with CO_2-independent L-15 media for the duration the cells are out and not actively being permeabilized. The cell dish is placed in a heated stage preheated to 37°C.

2) Cells were washed 2× with phosphate-buffered saline (PBS).

3) Cells were incubated with digitonin-RD2 cocktail for 8 min.

4) Cells were washed 2× with PBS.

5) We ensured that zero drift compensator on the microscope is active.

6) DOX $IC_{50} \times 10$ solution was added.

7) Two covers were replaced to ensure even heating.

8) Imaging process was started.

Note that $IC_{50} \times 10$ was required to get sufficient fluorescence in a 20-min time span for permeabilized cells. Unpermeabilized cells did not have any fluorescence over the experimental time. PC3 was subjected to the $IC_{50} \times 10$ of MDA-MB-231 cell line to standardize the dose that both cell lines were given.

Cell culture

MDA-MB-231 [female cancer line, American Type Culture Collection (ATCC), catalog no. HTB-26, RRID: $CVCL_0062$] was grown in complete media of Dulbecco's modified Eagle's medium (DMEM) and glucose (4.5 g/liter; Corning, catalog no. 10-013-CV) with 10% fetal bovine serum (FBS) and no antibiotics. PC3 (male cancer line, ATCC, catalog no. CRL-1435, RRID: $CVCL_0035$) was grown in complete media of RPMI 1640 (Gibco, catalog no. 11875-093) with 10% FBS and no antibiotics. Both cell lines would be passaged and plated onto an eight-well ibidi slide, where they would grow until they reach 80% confluence or greater and then would be used in a DOX uptake experiment. Cell lines were not explicitly verified using STR profiling and were not checked for mycoplasma contamination; however, the passage numbers of either cell line purchased directly through ATCC would not exceed passage number 8 for any experiment. Only the central four wells were used for dynamic DOX uptake studies to ensure near-identical well temperatures by the heated stage and ensure that DOX uptake was not modified by heated stage-based temperature fluctuations. All wells would be analyzed in 1 day to prevent infection risk. L-15 CO_2-independent and phenol red–free media (Gibco, catalog no. 21083-027) was used for a short duration (typically less than 1 hour) during the dox process for either cell line to prevent pH imbalance before permeabilization due to the open air gas exchange during the permeabilization process not being suitable for CO_2-dependent media in wells not being tested at that moment. Cells were not randomized, and the investigators were not blinded to the cell line during experiments.

Fixation and antibodies

For lamin A/C antibody staining, ice-cold acetone was used to fix and permeabilize the cells, incubated at −20° for 10 min. Cells were washed twice in PBS and then incubated for 10 min at room temperature on a shaker with 0.1% Triton X-100 and 0.5% bovine serum albumin (BSA) in PBS. Lamin A/C antibodies were purchased via Abcam (catalog no. ab205769, RRID: $AB_3105823$) and used at a concentration of 1:1000 for immunocytochemistry in conjunction with 0.1% Triton X-100 and 3% BSA for blocking for 1 hour at room temperature. Two washes were followed to remove nonspecifically bound antibodies with PBS, 0.1% Triton X-100, and 0.5% BSA before imaging. No counterstain was used to prevent fluorescence resonance energy transfering (FRETing). Nonreactive, carboxylic-acid Alexa Fluor 488 (Thermo Fisher Scientific, catalog no. A33077) control used for figs. S4 and S5. The same digitonin protocol was used (fig. S4) and a similar permeabilization protocol but replacing digitonin with streptolysin O (Millipore, catalog no. S5265) with a 15-min incubation time, similar to researchers Walev *et al.* (*35*) and Teng *et al.* (*70*) (fig. S5).

For dig. S6, cells were incubated with either 5 μM latrunculin or 10 μM nocodazole for 1 hour. Then, both control cells and treated cells were fixed with PFA for 20 min at room temperature. Cells were then washed twice with PBS and incubated for 10 min with a perm buffer (0.1% Triton X-100 and 0.5% BSA in PBS) at room temperature on a shaker. Then, the cells were incubated with 0.1% Triton X-100, 3% BSA, RD2, phalloidin 594, and α tubulin antibody in PBS for 30 min at room temperature on a shaker. The cells were then washed twice before imaging.

For α tubulin antibody staining shown in fig. S11, after digitonin permeabilization, both control cells and permeabilized cells were fixed with PFA for 30 min. The use of PFA over acetone was to ensure that fixation happened before further permeabilization of the cell membrane, as acetone is known to do both simultaneously, and we wished to ensure that nonpermeabilized control cells maintained all cytoskeletal structure as comparison in case permeabilization disrupted that. Cells were then washed twice with PBS and then incubated for 10 min at room temperature on a shaker with 0.1% Triton X-100 and 0.5% BSA in PBS. α Tubulin antibody was purchased from Thermo Fisher Scientific (Thermo Fisher Scientific, catalog no. 53-4502-82, RRID: $AB_1210525$) and used at a concentration of 1:100 in conjunction with 0.1% Triton X-100, 3% BSA, and phalloidin 594 (AAT Bioquest, catalog no. 23122) for blocking for 1 hour at room temperature on a shaker. Two washes with permeabilization buffer were used to remove nonspecific bound antibody and phalloidin, before RD2, the nuclear stain dye, was introduced for 10 min and then washed.

Confocal microscopy of nuclear uptake and antibody staining

An Olympus FluoView FV3000 (RRID: SCR_017015) was used for all imaging purposes, and a Pecon TempController 2000-2 was used to ensure an adequate body temperature was maintained throughout the entirety of the experiment. For live-cell DOX experiments, microscope settings were maintained across cell lines and conditions, and DOX was excited using the 488 laser line at 2% power and 600 HV and captured using a filter that allows 570- to 620-nm wavelength light to pass through to prevent significant photobleaching over the span of 20 min, where an image was taken every 6.43 s. Simultaneous imaging of DOX and RD2 was possible due to the excitation and emission differences, where RD2 was excited at 640, its fluorescence was captured at 657 to 757 nm with a laser power of 4.5% and an HV of 700, and all images were taken using a 20× air UPlanSapo 0.75 NA and a resolution size of 1024 × 1024. Similarly, the Alexa studies used 1.5% laser power and 400 HV and captured using a filter that allows 500- to 540-nm wavelength light at the same imaging interval for the data in figs. S4 and S5 (right). For fig. S5 (left), where the timespan was 45 s, images were taken every 0.5 s for Alexa and high concentration DOX. The same objective was used for all Alexa, RD2, and DOX time-lapse studies. The Olympus ZDC autofocus unit was used for all time-lapse imaging studies to ensure the same focal plane was studied.

For lamin studies used a 488 laser line to excite at a power of 5% and an HV of 525, collecting a z-stack throughout the entire thickness of the nuclei in the field of view to ensure that nuclei at different heights were accounted for without bias. No nucleus counter stain was used to ensure that FRETing did not occur to any extent, as DRAQ5 made fluorescence slightly weaker. These images were taken using a 40× air UPlanSapo 0.95 NA and an image size of 1024 × 1024. For purified nuclei studies, DOX/RD2 laser power and image acquisition rate were changed due to a faster uptake because the cytoplasm is not existent. DOX was excited using the 488 laser line at 1% power and 600 HV and captured using a filter that allows 570 to 620 nm wavelength light to pass through, while RD2 used a 640 laser line at 3% laser power and 600 HV for a filter of 657 to 757 nm using the 20× air UPlanSapo 0.75 NA and an image size of 1024 × 1024. For the purified nuclei blebbistatin crowding control in fig. S19, a static image was taken, and RD2 (640 laser line 1.5% power, 600 HV, and a filter of 650 to 750 nm) and blebbistatin (445 laser line, 50% power, 750 HV, and a filter of 460 to 500 nm) were taken sequentially using the 20× air UPlanSapo 0.75 NA and a resolution size of 1024 × 1024.

siRNA reverse transfection protocol

On the basis of titration experiments to optimize Lipofectamine and siRNA concentrations, 0.75 μl of Lipofectamine RNAiMAX (Invitrogen, catalog no. 13778-030) and 25 nM oLMNA (Ambion, catalog no. 4390824) or Scramble (Ambion, catalog no. 4390843) siRNA were used for these experiments.

For four wells combined:

1) 8.4 μl (equates to 6 pmol of RNAiDuplex) solution of the siRNA (invert if thawing) was mixed to 160 μl of Opti-MEM media with reduced serum.

2) One quarter of the volume was placed in each well that the cells will be seeded into and mixed gently.

3) Lipofectamine was inverted, and 0.75 μl of Lipofectamine RNAiMax was added to each well, mixed gently, and incubated for 20 min.

4) Cells were diluted in complete growth medium without antibiotics. The final volume for 60 to 80% coverage at 24 hours of plating should be 200 μl of media per well.

5) The 200 μl of cell-media mixture was added to each well containing the RNA solution and mixed gently by rocking back and forth.

6) The media + cells + RNA solution were incubated for 24 to 72 hours (the transfection time) at 37°C depending on protein half-life.

7) Media was replaced after 24 hours past transfection time.

Cytoskeletal treatments

All cytoskeletal inhibition solutions were used in conjunction with complete growing media DMEM glucose (4.5 g/liter) and incubated with MDA-MB-231 cells, but times and concentrations vary based on previous researchers effective concentrations. Nocodazole (Millipore, catalog no. 487929) (10 μM), and latrunculin A (STEMCELL Technologies, catalog no. 100-0563) (5 μM) solutions were incubated for 1 hour as per Aspengren *et al.* (*50*). Blebbistatin (Millipore, catalog no. 203389) (10 μM) was also incubated for 1 hour with cells in darkness to ensure inhibition of myosin II as per Farman *et al.* (*51*). Acrylamide (VWR, catalog no. 0341) was the least acute treatment, where a 10 mM solution was incubated with cells for 2 hours to interrupt cytoskeletal filaments, as was previously shown by Arocena (*52*). Verapamil (in kit from Biotium, catalog no. 40081) concentrations (10 μM) and incubation times (30 min) were influenced by biotium's NucSpot-488 (Biotium, catalog no. 40081) protocol and Roger *et al.* (*71*) protocol that used MDA-MB-231 in conjunction with verapamil.

Purification of nuclei

A detergent-free nuclei isolation kit (Invent biotechnologies catalog no. NI-024) was used to extract intact nuclei from cells following their posted protocol. Nuclei were never frozen and refrigerated for a minimum of 0 days and a maximum of 2 days before being used for any study. To be used in any uptake study, nuclei were first attached to sterile ibidi eight-well slides that had been pretreated with polylysine-L to help nuclei attach. They were then spun down onto the slides at 450*g* for 5 min, following a similar protocol in Neely and Bao (*37*). Then, the nuclei were prestained with RD2 for 10 min followed by two PBS washes and kept hydrated for ease of fluorescent visualization. After a plane and field of view were found, the DOX study proceeded similarly to what was shown above for the digitonin protocol, but without the digitonin step (effectively starting at step 5 of the digitonin protocol).

Image processing ImageJ

Post-processing was done through ImageJ (version 2.14.0,RRID: $SCR_0$03070), where images where background was subtracted, and then the image was blurred to create an ideal gray image for autothresholding. Autothresholding used the Otsu method to identify nuclear objects, and two populations were captured using the autothresholding method a second time while ignoring the extra bright nuclei that were captured during the first autothresholding object detection. A macro script was built to allow for the same process to be used across cell lines and treatments, reducing bias while obtaining a very high capture rate of both of the different nuclei populations, (see fig. S21 for examples of segmentation protocol). Creating three populations was explored, but background and cytosol were regularly captured in the third, indicating that there was not a significant population of nuclei that were not captured in steps 1 and 2.

MATLAB analysis

Figures 2 (C and D), 3C, 4 (B and C), and 5 (B and C) were using the total amount of nuclei in all fields of view, where the range of fluorescence was the maximum-minimum fluorescence on a per nuclei basis. $V_{Nuclear}$ was obtained after a multistep process. First, we interpolated both time and DOX uptake F.I. to obtain a greater number of data points and then fit the interpolated data to a Savitzky-Golay filter to reduce any noise-based oscillations. Then, the slope of the Savitzky-Golay filtered data was obtained at every time step, and the maximum slope was used as the metric for $V_{Nuclear}$ or the maximum rate of nuclear entry. Both $V_{Nuclear}$ and total range of fluorescence for all individual nuclei over all fields of view/experiments were then pooled together, and the medians and quartiles were obtained and highlighted in a graphical form, as well as nonparametric statistics were completed to compare these non-normal populations. All statistical analyses were using nonparametric statistics such as Kruskal-Wallis analysis of variance (ANOVA) for studies that had more than two populations that were compared and Mann-Whitney *U* tests for studies that had exactly two populations to compare.

Clustering seen in fig. S20 was done by fitting the F.I. and circularity scatter plots with a Gaussian mixture model, where the number of components were two, indicating, based on the scatter plot–separated clusters, that two subpopulations exist within a single-cell population. After a Gaussian fit has been completed, the cluster function was called to separate the population into the two components to be further analyzed.

Supplementary Materials

The PDF file includes:

Figs. S1 to S21
Tables S1 to S9
Legends for movies S1 to S4
References

Other Supplementary Material for this manuscript includes the following:

Movies S1 to S4

REFERENCES AND NOTES

1. M. T. Amjad, A. Chidharla, A. Kasi, *Cancer Chemotherapy* (StatPearls Publishing, 2022).
2. S. K. Gupta, P. Singh, V. Ali, M. Verma, Role of membrane-embedded drug efflux abc transporters in the cancer chemotherapy. *Oncol Rev.* **14**, 448 (2020).
3. F. Michor, M. A. Nowak, Y. Iwasa, Evolution of resistance to cancer therapy. *Curr. Pharm. Des.* **12**, 261–271 (2006).

4. Y.-Y. Liu, T.-Y. Han, A. E. Giuliano, M. C. Cabot, Ceramide glycosylation potentiates cellular multidrug resistance. *FASEB J.* **15**, 719–730 (2001).
5. J. Zhou, C.-Y. Wang, T. Liu, B. Wu, F. Zhou, J.-X. Xiong, H.-S. Wu, J. Tao, G. Zhao, M. Yang, S. M. Gou, Persistence of side population cells with high drug efflux capacity in pancreatic cancer. *World J. Gastroenterol.* **14**, 925–930 (2008).
6. Y. Kinoshita, T. Kalir, J. Rahaman, P. Dottino, D. S. Kohtz, Alterations in nuclear pore architecture allow cancer cell entry into or exit from drug-resistant dormancy. *Am. J. Pathol.* **180**, 375–389 (2012).
7. M. El-Tanani, E.-H. Dakir, B. Raynor, R. Morgan, Mechanisms of nuclear export in cancer and resistance to chemotherapy. *Cancer* **8**, 35 (2016).
8. N. R. Scott, S. H. Parekh, A-type lamins involvement in transport and implications in cancer? *Nucleus* **13**, 223–237 (2022).
9. A. García-González, E. Jacchetti, R. Marotta, M. Tunesi, J. F. R. Matas, M. T. Raimondi, The effect of cell morphology on the permeability of the nuclear envelope to diffusive factors. *Front. Physiol.* **9**, 925 (2018).
10. L. J. Colwell, M. P. Brenner, K. Ribbeck, Charge as a selection criterion for translocation through the nuclear pore complex. *PLoS Comput. Biol.* **6**, e1000747 (2010).
11. G. Batist, J. Barton, P. Chaikin, C. Swenson, L. Welles, Myocet (liposome-encapsulated doxorubicin citrate): A new approach in breast cancer therapy. *Expert Opin. Pharmacother.* **3**, 1739–1751 (2002).
12. R. Sawpari, S. Samanta, J. Banerjee, S. Das, S. S. Dash, R. Ahmed, B. Giri, S. K. Dash, Recent advances and futuristic potentials of nano-tailored doxorubicin for prostate cancer therapy. *J. Drug Deliv. Technol.* **81**, 104212 (2023).
13. B. Guo, H.-L. Zhu, S.-X. Li, X.-C. Lu, H. Fan, Individualized liposomal doxorubicin-based treatment in elderly patients with non-hodgkin's lymphoma. *Oncol Res. Treat.* **34**, 184–188 (2011).
14. A. Ruggiero, G. De Rosa, D. Rizzo, A. Leo, P. Maurizi, A. De Nisco, F. Vendittelli, C. Zuppi, A. Mordente, R. Riccardi, Myocardial performance index and biochemical markers for early detection of doxorubicin-induced cardiotoxicity in children with acute lymphoblastic leukaemia. *Int. J. Clin. Oncol.* **18**, 927–933 (2013).
15. A.-M. Meredith, C. R. Dass, Increasing role of the cancer chemotherapeutic doxorubicin in cellular metabolism. *J. Pharm. Pharmacol.* **68**, 729–741 (2016).
16. N.-T. Chen, C.-Y. Wu, C.-Y. Chung, Y. Hwu, S.-H. Cheng, C.-Y. Mou, L.-W. Lo, Probing the dynamics of doxorubicin-dna intercalation during the initial activation of apoptosis by fluorescence lifetime imaging microscopy (flim). *PLOS ONE* **7**, e44947 (2012).
17. J. L. Nitiss, Investigating the biological functions of dna topoisomerases in eukaryotic cells. *Biochim. Biophys. Acta* **1400**, 63–81 (1998).
18. I. Micallef, B. Baron, Doxorubicin: An overview of the anti-cancer and chemoresistance mechanisms. *Ann. Clin. Toxicol.* **3**, 1031 (2020).
19. H. Keizer, H. Pinedo, G. Schuurhuis, H. Joenje, Doxorubicin (adriamycin): A critical review of free radical-dependent mechanisms of cytotoxicity. *Pharmacol. Ther.* **47**, 219–231 (1990).
20. L. Chin, Y. Xia, D. E. Discher, P. A. Janmey, Mechanotransduction in cancer. *Curr. Opin. Chem. Eng.* **11**, 77–84 (2016).
21. F. Broders-Bondon, T. H. N. Ho-Bouldoires, M.-E. Fernandez-Sanchez, E. Farge, Mechanotransduction in tumor progression: The dark side of the force. *J. Cell Biol.* **217**, 1571–1587 (2018).
22. S. Liu, Y. Li, Y. Hong, M. Wang, H. Zhang, J. Ma, K. Qu, G. Huang, T. J. Lu, Mechanotherapy in oncology: Targeting nuclear mechanics and mechanotransduction. *Adv. Drug Deliv. Rev.* **194**, 114722 (2023).
23. J. Lammerding, P. C. Schulze, T. Takahashi, S. Kozlov, T. Sullivan, R. D. Kamm, C. L. Stewart, R. T. Lee, Lamin A/C deficiency causes defective nuclear mechanics and mechanotransduction. *J. Clin. Invest.* **113**, 370–378 (2004).
24. S. Mishra, D. L. Levy, Nuclear f-actin and lamin a antagonistically modulate nuclear shape. *J. Cell Sci.* **135**, jcs259692 (2022).
25. I. F. Rizzuti, P. Mascheroni, S. Arcucci, Z. Ben-Mériem, A. Prunet, C. Barentin, C. Rivière, H. Delanoë-Ayari, H. Hatzikirou, J. Guillermet-Guibert, M. Delarue, Mechanical control of cell proliferation increases resistance to chemotherapeutic agents. *Phys. Rev. Lett.* **125**, 128103 (2020).
26. P. Mascheroni, D. Boso, L. Preziosi, B. A. Schrefler, Evaluating the influence of mechanical stress on anticancer treatments through a multiphase porous media model. *J. Theor. Biol.* **421**, 179–188 (2017).
27. Y. Fan, Q. Sun, X. Li, J. Feng, Z. Ao, X. Li, J. Wang, Substrate stiffness modulates the growth, phenotype, and chemoresistance of ovarian cancer cells. *Front. Cell. Dev. Biol.* **9**, 718834 (2021).
28. J. M. Northcott, I. S. Dean, J. K. Mouw, V. M. Weaver, Feeling stress: The mechanics of cancer progression and aggression. *Front. Cell Dev. Biol.* **6**, 17 (2018).
29. P. Papageorgis, C. Polydorou, F. Mpekris, C. Voutouri, E. Agathokleous, C. P. Kapnissi-Christodoulou, T. Stylianopoulos, Tranilast-induced stress alleviation in solid tumors improves the efficacy of chemo-and nanotherapeutics in a size-independent manner. *Sci. Rep.* **7**, 46140 (2017).
30. S. Wang, N. G. Perkins, F. Ji, R. Chaudhuri, Z. Guo, P. Sarkar, S. Shao, Z. Li, M. Xue, Digitonin-facilitated delivery of imaging probes enables single-cell analysis of akt signalling activities in suspension cells. *Analyst* **146**, 5307–5315 (2021).
31. J. E. Hagstrom, J. J. Ludtke, M. C. Bassik, M. G. Sebestyén, S. A. Adam, J. A. Wolff, Nuclear import of dna in digitonin-permeabilized cells. *J. Cell Sci.* **110**, 2323–2331 (1997).
32. J. Liu, N. Xiao, D. B. DeFranco, Use of digitonin-permeabilized cells in studies of steroid receptor subnuclear trafficking. *Methods* **19**, 403–409 (1999).
33. S. A. Adam, R. S. Marr, L. Gerace, Nuclear protein import in permeabilized mammalian cells requires soluble cytoplasmic factors. *J. Cell Biol.* **111**, 807–816 (1990).
34. N. Nitin, L. LaConte, W. J. Rhee, G. Bao, Tat peptide is capable of importing large nanoparticles across nuclear membrane in digitonin permeabilized cells. *Ann. Biomed. Eng.* **37**, 2018–2027 (2009).
35. I. Walev, S. C. Bhakdi, F. Hofmann, N. Djonder, A. Valeva, K. Aktories, S. Bhakdi, Delivery of proteins into living cells by reversible membrane permeabilization with streptolysin-o. *Proc. Natl. Acad. Sci. U.S.A.* **98**, 3185–3190 (2001).
36. S. A. Adam, R. Sterne-Marr, L. Gerace, In vitro nuclear protein import using permeabilized mammalian cells. *Methods Cell Biol.* **35**, 469–482 (1991).
37. A. E. Neely, X. Bao, Nuclei isolation staining (nis) method for imaging chromatin-associated proteins in difficult cell types. *Curr. Protoc. Cell Biol.* **84**, e94 (2019).
38. E. Tsakalozou, A. M. Eckman, Y. Bae, Combination effects of docetaxel and doxorubicin in hormone-refractory prostate cancer cells. *Biochem. Res. Int.* **2012**, 1–10 (2012).
39. S.-H. Wen, S.-C. Su, B.-H. Liou, C.-H. Lin, K.-R. Lee, Sulbactam-enhanced cytotoxicity of doxorubicin in breast cancer cells. *Cancer Cell Int.* **18**, 1–18 (2018).
40. M. A. D'Angelo, J. S. Gomez-Cavazos, A. Mei, D. H. Lackner, M. W. Hetzer, A change in nuclear pore complex composition regulates cell differentiation. *Dev. Cell* **22**, 446–458 (2012).
41. A. Garcia, J. F. R. Matas, M. T. Raimondi, Modeling of the mechano-chemical behaviour of the nuclear pore complex: current research and perspectives. *Integr. Biol.* **8**, 1011–1021 (2016).
42. I. Andreu, I. Granero-Moya, N. R. Chahare, K. Clein, M. Molina-Jordán, A. E. Beedle, A. Elosegui-Artola, J. F. Abenza, L. Rossetti, X. Trepat, B. Raveh, P. Roca-Cusachs, Mechanical force application to the nucleus regulates nucleocytoplasmic transport. *Nat. Cell Biol.* **24**, 896–905 (2022).
43. M. J. Mitchell, M. R. King, Fluid shear stress sensitizes cancer cells to receptor-mediated apoptosis via trimeric death receptors. *New J. Phys.* **15**, 015008 (2013).
44. L. M. Hoffman, M. A. Smith, C. C. Jensen, M. Yoshigi, E. Blankman, K. S. Ullman, M. C. Beckerle, Mechanical stress triggers nuclear remodeling and the formation of transmembrane actin nuclear lines with associated nuclear pore complexes. *Mol. Biol. Cell* **31**, 1774–1787 (2020).
45. F. A. Pennacchio, P. Nastały, A. Poli, P. Maiuri, Tailoring cellular function: the contribution of the nucleus in mechanotransduction. *Front. Bioeng. Biotechnol.* **8**, 596746 (2021).
46. M. M. Nava, R. Fedele, M. T. Raimondi, Computational prediction of strain-dependent diffusion of transcription factors through the cell nucleus. *Biomech. Model. Mechanobiol.* **15**, 983–993 (2016).
47. B. L. Timney, B. Raveh, R. Mironska, J. M. Trivedi, S. J. Kim, D. Russel, S. R. Wente, A. Sali, M. P. Rout, Simple rules for passive diffusion through the nuclear pore complex. *J. Cell Biol.* **215**, 57–76 (2016).
48. L. Kong, G. Schäfer, H. Bu, Y. Zhang, Y. Zhang, H. Klocker, Lamin A/C protein is overexpressed in tissue-invading prostate cancer and promotes prostate cancer cell growth, migration and invasion through the pi3k/akt/pten pathway. *Carcinogenesis* **33**, 751–759 (2012).
49. N. Wang, J. D. Tytell, D. E. Ingber, Mechanotransduction at a distance: Mechanically coupling the extracellular matrix with the nucleus. *Nat. Rev. Mol. Cell Biol.* **10**, 75–82 (2009).
50. S. Aspengren, L. Wielbass, M. Wallin, Effects of acrylamide, latrunculin, and nocodazole on intracellular transport and cytoskeletal organization in melanophores. *Cell Motil. Cytoskeleton* **63**, 423–436 (2006).
51. G. P. Farman, K. Tachampa, R. Mateja, O. Cazorla, A. Lacampagne, P. P. de Tombe, Blebbistatin: Use as inhibitor of muscle contraction. *Pflugers Arch.* **455**, 995–1005 (2008).
52. M. Arocena, Effect of acrylamide on the cytoskeleton and apoptosis of bovine lens epithelial cells. *Cell Biol. Int.* **30**, 1007–1012 (2006).
53. N. T. Wakhloo, S. Anders, F. Badique, M. Eichhorn, I. Brigaud, T. Petithory, M. Vassaux, J.-L. Milan, J.-N. Freund, J. Rühe et al., Actomyosin, vimentin and linc complex pull on osteosarcoma nuclei to deform on micropillar topography. *Biomaterials* **234**, 119746 (2020).
54. J. Lammerding, L. G. Fong, J. Y. Ji, K. Reue, C. L. Stewart, S. G. Young, R. T. Lee, Lamins A and C but not lamin B1 regulate nuclear mechanics. *J. Biol. Chem.* **281**, 25768–25780 (2006).
55. M. M. Mukaka, A guide to appropriate use of correlation coefficient in medical research. *Malawi Med. J.* **24**, 69–71 (2012).

56. S. Groeger, Y. Wang, S. Ruf, L. Wang, The dual roles of lamin A/C in mechanosensation to compressive force (Research Square, 2023).
57. N. Lamm, M. N. Read, M. Nobis, D. Van Ly, S. G. Page, V. P. Masamsetti, P. Timpson, M. Biro, A. J. Cesare, Nuclear f-actin counteracts nuclear deformation and promotes fork repair during replication stress. *Nat. Cell Biol.* **22**, 1460–1470 (2020).
58. N. C. Kampan, M. T. Madondo, O. M. McNally, M. Quinn, M. Plebanski et al., Paclitaxel and its evolving role in the management of ovarian cancer. *Biomed. Res. Int.* **2015**, 413076 (2015).
59. K. S. Kim, C. H. Cho, E. K. Park, M.-H. Jung, K.-S. Yoon, H.-K. Park, Afm-detected apoptotic changes in morphology and biophysical property caused by paclitaxel in ishikawa and hela cells. *PLOS ONE* **7**, e30066 (2012).
60. M. Kiwanuka, G. Higgins, S. Ngcobo, J. Nagawa, D. M. Lang, M. H. Zaman, N. H. Davies, T. Franz, Effect of paclitaxel treatment on cellular mechanics and morphology of human oesophageal squamous cell carcinoma in 2D and 3D environments. *Integr. Biol.* **14**, 137–149 (2022).
61. E. R. Smith, J. Leal, C. Amaya, B. Li, X.-X. Xu, Nuclear lamin A/C expression is a key determinant of paclitaxel sensitivity. *Mol. Cell. Biol.* **41**, e00648-20 (2021).
62. A. A. Sprouse, B.-S. Herbert, Resveratrol augments paclitaxel treatment in mda-mb-231 and paclitaxel-resistant mda-mb-231 breast cancer cells. *Anticancer Res* **34**, 5363–5374 (2014).
63. D. Mohr, S. Frey, T. Fischer, T. Güttler, D. Görlich, Characterisation of the passive permeability barrier of nuclear pore complexes. *EMBO J.* **28**, 2541–2553 (2009).
64. M. S. Poruchynsky, E. Komlodi-Pasztor, S. Trostel, J. Wilkerson, M. Regairaz, Y. Pommier, X. Zhang, T. Kumar Maity, R. Robey, M. Burotto, D. Sackett, U. Guha, A. T. Fojo, Microtubule-targeting agents augment the toxicity of DNA-damaging agents by disrupting intracellular trafficking of dna repair proteins. *Proc. Natl. Acad. Sci. U.S.A.* **112**, 1571–1576 (2015).
65. S. Maynard, G. Keijzers, M. Akbari, M. B. Ezra, A. Hall, M. Morevati, M. Scheibye-Knudsen, S. Gonzalo, J. Bartek, V. A. Bohr, Lamin A/C promotes DNA base excision repair. *Nucleic Acids Res.* **47**, 11709–11728 (2019).
66. A. W. Cook, C. P. Toseland, The roles of nuclear myosin in the DNA damage response. *J. Biochem.* **169**, 265–271 (2021).
67. M. W. Lambert, The functional importance of lamins, actin, myosin, spectrin and the linc complex in DNA repair. *Exp. Biol. Med.* **244**, 1382–1406 (2019).
68. G. W. Sledge, D. Neuberg, P. Bernardo, J. N. Ingle, S. Martino, E. K. Rowinsky, W. C. Wood, Phase III trial of doxorubicin, paclitaxel, and the combination of doxorubicin and paclitaxel as front-line chemotherapy for metastatic breast cancer: An intergroup trial (e1193). *J. Clin. Oncol.* **21**, 588–592 (2003).
69. N. Wang, Review of cellular mechanotransduction. *J. Phys. D Appl. Phys.* **50**, 233002 (2017).
70. K. W. Teng, P. Ren, P. R. Selvin, Delivery of fluorescent probes using streptolysin o for fluorescence microscopy of living cells. *Curr. Protoc. Protein Sci.* **93**, e60 (2018).
71. S. Roger, J.-Y. L. Guennec, P. Besson, Particular sensitivity to calcium channel blockers of the fast inward voltage-dependent sodium current involved in the invasive properties of a metastastic breast cancer cell line. *Br. J. Pharmacol.* **141**, 610–615 (2004).
72. M. J. H. Geelen, The use of digitonin-permeabilized mammalian cells for measuring enzyme activities in the course of studies on lipid metabolism. *Analytical Biochemistry*, **347**, 1–9 (2005); https://doi.org/10.1016/j.ab.2005.03.032.

Acknowledgments

Funding: We thank S.H.P. laboratory for support in this work. N.R.S. acknowledges THRUST 2000 and Temple Foundation Graduate Fellowships from the Cockrell School of Engineering. S.H.P. acknowledges support from the Welch Foundation (F-2008-20220331), the National Science Foundation (no. 2146549), Texas 4000 funding, and the National Cancer Institute, National Institutes of Health, under contract no.75N91019D00024, task order no. 75N91020F00003. The content of this publication does not necessarily reflect the views or policies or imply endorsement by the US Government or any other funding body. **Author contributions:** N.S.: Writing—original draft, conceptualization, investigation, writing—review and editing, methodology, resources, data curation, validation, formal analysis, software, project administration, and visualization. S.K.: Writing—original draft, investigation, and formal analysis. S.H.P.: Writing—original draft, conceptualization, methodology, resources, funding acquisition, validation, supervision, project administration, and visualization. **Competing interests:** The authors declare that they have no competing interests. **Data and materials availability:** All data needed to evaluate the conclusions in the paper are present in the paper and/or the Supplementary Materials.

Submitted 9 July 2024
Accepted 14 November 2024
Published 18 December 2024
10.1126/sciadv.adr5947